

**NAVAL POSTGRADUATE SCHOOL**  
**Monterey, California**



**THESIS**

**A DISCRETE, DIGITAL FILTER FOR FORWARD  
PREDICTION OF SEAWAY ELEVATION RESPONSE**

by

Anthony L. Simmons

March 1997

Thesis Advisor:

Anthony J. Healey

**Approved for public release; distribution is unlimited.**

DTIC QUALITY INSPECTED 3

19971121 126

# REPORT DOCUMENTATION PAGE

Form Approved  
OMB No. 0704-0188

wazzu Public reporting burden for this collection of information is estimated to average 1 hour per response, including the time for reviewing instruction, searching existing data sources, gathering and maintaining the data needed, and completing and reviewing the collection of information. Send comments regarding this burden estimate or any other aspect of this collection of information, including suggestions for reducing this burden, to Washington headquarters Services, Directorate for Information Operations and Reports, 1215 Jefferson Davis Highway, Suite 1204, Arlington, VA 22202-4302, and to the Office of Management and Budget, Paperwork Reduction Project (0704-0188) Washington DC 20503.

1. AGENCY USE ONLY (Leave blank)		2. REPORT DATE March 1997	3. REPORT TYPE AND DATES COVERED Master's Thesis
4. TITLE AND SUBTITLE: A DISCRETE, DIGITAL FILTER FOR FORWARD PREDICTION OF SEAWAY ELEVATION RESPONSE			5. FUNDING NUMBERS
6. AUTHOR(S): Anthony L. Simmons			
7. PERFORMING ORGANIZATION NAME(S) AND ADDRESS(ES) Naval Postgraduate School Monterey, CA 93943-5000			8. PERFORMING ORGANIZATION REPORT NUMBER
9. SPONSORING / MONITORING AGENCY NAME(S) AND ADDRESS(ES)			10. SPONSORING / MONITORING AGENCY REPORT NUMBER
11. SUPPLEMENTARY NOTES The views expressed in this thesis are those of the author and do not reflect the official policy or position of the Department of Defense or the U.S. Government.			
12a. DISTRIBUTION / AVAILABILITY STATEMENT Approved for public release; distribution unlimited.			12b. DISTRIBUTION CODE
13. ABSTRACT (maximum 200 words)  The Autonomous Underwater Vehicle (AUV) must be able to operate in various shallow water sea state conditions. In order to have a precise navigation and steering system, and efficiently place charges on underwater mines, the AUV must be able to sense and overcome hydrodynamic forces which are caused by waves. This thesis establishes a model of sea state conditions based on spectral analysis, and uses the model to predict future knowledge of the sea. This prediction is determined by the random white noise output of a discrete, digital filter. The development of the discrete, digital filter is described herein. The Pierson-Moskowitz (P-M) spectrum which models seaway elevations using linear wave theory is used as a target spectrum which the filter will track. Cross-correlation between the P-M target spectrum and digital filter have shown that a reasonably accurate estimate of wave elevations can be predicted one full wave period into the future.			
14. SUBJECT TERMS AUV, Autonomous Underwater Vehicle, Mine Warfare			15. NUMBER OF PAGES 83
			16. PRICE CODE
17. SECURITY CLASSIFICATION OF REPORT Unclassified	18. SECURITY CLASSIFICATION OF THIS PAGE Unclassified	19. SECURITY CLASSIFICATION OF ABSTRACT Unclassified	20. LIMITATION OF ABSTRACT UL

NSN 7540-01-280-5500

Standard Form 298 (Rev. 2-89)  
Prescribed by ANSI Std. Z39-18

DRIG QUALITY CONTROL



Approved for public release; distribution is unlimited

**A DISCRETE, DIGITAL FILTER FOR FORWARD PREDICTION OF SEAWAY  
ELEVATION RESPONSE**

Anthony L. Simmons  
Lieutenant, United States Navy  
B.S., Austin Peay State University, 1989

Submitted in partial fulfillment of the  
requirements for the degree of

**MASTER OF SCIENCE IN MECHANICAL ENGINEERING**

from the

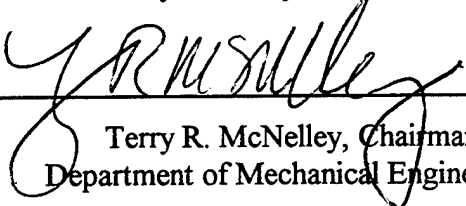
**NAVAL POSTGRADUATE SCHOOL  
March 1997**

Author:

  
\_\_\_\_\_  
Anthony L. Simmons

Approved by:

  
\_\_\_\_\_  
Anthony J. Healey, Thesis Advisor

  
\_\_\_\_\_  
Terry R. McNelley, Chairman  
Department of Mechanical Engineering



## ABSTRACT

The Autonomous Underwater Vehicle (AUV) must be able to operate in various shallow water sea state conditions. In order to have a precise navigation and steering system, and efficiently place charges on underwater mines, the AUV must be able to sense and overcome hydrodynamic forces which are caused by waves. This thesis establishes a model of sea state conditions based on spectral analysis, and uses the model to predict future knowledge of the sea. This prediction is determined by the random white noise output of a discrete, digital filter. The development of the discrete, digital filter is described herein. The Pierson-Moskowitz (P-M) spectrum which models seaway elevations using linear wave theory is used as a target spectrum which the filter will track. Cross-correlation between the P-M target spectrum and digital filter have shown that a reasonably accurate estimate of wave elevations can be predicted one full wave period into the future.



## TABLE OF CONTENTS

I.	INTRODUCTION . . . . .	1
	A. HISTORY ON MINE COUNTERMEASURES . . . . .	1
	B. MINEHUNTING IN SHALLOW WATER (10 TO 40 FEET) . . . . .	1
	C. DISTURBANCE REJECTION . . . . .	2
	D. OBJECTIVE OF THESIS . . . . .	3
II.	LINEAR PREDICTION THEORY (LPT) . . . . .	5
	A. HISTORY AND FORMULATION OF LPT . . . . .	5
	B. MODELING OF THE SYSTEM AND REAL TIME-FORWARD PREDICTION . . . . .	15
	C. PROBLEMS ENCOUNTERED WHEN USING LINEAR PREDICTION THEORY . . . . .	24
III.	APPLICATION TO WAVE MOTION PREDICTION . . . . .	25
	A. PIERSON-MOSKOWITZ (P-M) SPECTRUM . . . . .	25
	B. PIERSON-MOSKOWITZ (P-M) AND PRESSUE PROFILE TARGET SPECTRUM . . . . .	26
	C. SPANOS' DIMENSIONLESS ARMA FILTER . . . . .	34
	D. EIGHTH-ORDER FILTER . . . . .	37
IV.	RESULTS . . . . .	51
V.	CONCLUSION AND RECOMMENDATIONS . . . . .	67

A. CONCLUSION . . . . .	67
B. RECOMMENDATIONS . . . . .	68
LIST OF REFERENCES . . . . .	69
APPENDIX: EIGHTH-ORDER FILTER . . . . .	71
INITIAL DISTRIBUTION LIST . . . . .	73

## **I. INTRODUCTION**

### **A. HISTORY ON MINE APPROXIMATION COUNTERMEASURES**

Once the Navy's primary mission shifted from "Sea Control" (blue water operations) to "From the Sea" (shallow water operations), the increased requirement for amphibious warfare operations demanded that increased interest be placed in the area of mine countermeasures - specifically, mine warfare in shallow water. Because of the immense level of tension and somewhat frequent conflicts recently arising in the Middle East, the interest of the United States security has often been channeled toward the mine infested waters of the Arabian Gulf. Over the past ten years or so, the United States has discovered and cleared a large number of underwater mines in this area. Furthermore, there have been some adverse developments occur as an aftermath of ships encountering explosive mines. To this end, we must continuously remain attentive of this phenomenal threat to our forces and continue , to seek improvement toward measures of combating this hostile and unwavering enemy by devising safe and efficient tools to prevent mines from presenting future problems, and hindering the effective operation of Amphibious Warfare.

As a measure to alleviate the danger of underwater mines, the Naval Postgraduate School Center for Autonomous Underwater Vehicle (AUV) Research through Mechanical, Electrical Engineering, and Computer Science Departments are continuously researching new methods to overcome this ongoing challenge.

### **B. MINEHUNTING IN SHALLOW WATER (10 TO 40 FEET)**

With the new mission (From the Sea) in place, today's Modern Navy, more than ever before has focused on means to intelligently and efficiently counter the challenge presented by floating mines by employing countermeasures in shallow water. Mine hunting in shallow water has presented continuous challenges to the safe and effective

operation of the United States Naval Forces. For maximum flexibility the mine countermeasure efforts should be covert, cost effective and relatively quick, (Richwine, 1995). The countermeasure methods currently used by Naval Forces include the involvement of humankind, noisy platforms such as ships and helicopters. These aforementioned methods require a high risk of human sacrifice, and compromises covertness respectively. As another measure, marine mammal systems and special military forces are capable of operating covertly. However, they are scarce resources that require extensive training pipelines, (Hunt, 1995).

Owing to the robust advancement in technology, countermeasures using autonomous systems are currently being built and tested at the Naval Postgraduate School. In previous studies at the Navy Postgraduate school, an autonomous underwater vehicle (Phoenix) has been developed and operated in a test tanks where sea state conditions were negligible. In order to advance the studies and operability of the AUV, wave and current forces must be considered and incorporated in the test environment.

### **C. DISTURBANCE REJECTION**

The main source of the dynamic forces encountered by underwater vehicles or submerged vessels are wave and current induced. These disturbance forces arise from buoyant and inertial effects due to ocean wave kinematics. In the past, most sea state models were predicted using an ergodic process. To best assess the performance of an AUV in shallow water, it is necessary to generate a dynamic model of the velocity and acceleration particles of water to model the wave forces. Although frequency decomposition is a well known method to simulate time history variation of the ocean surface due to waves, the digital representation of the sea surface elevation and pressure profile process was thought to offer advantages, and is referred to as a time series of wave history. Because there is a strong uncertainty of random ocean wave fields, in the past, a spectral approach has been best suited for describing the intensity and frequency characteristics of ocean wave fields.

Recent research on simulating ocean disturbance was conducted by Spanos during the an Offshore Structures Conference, (Spanos and Mignolet, 1986). His research expanded on the use of the Linear Prediction Theory using Autoregressive (AR) and Autoregressive Moving Average (ARMA) Models. With the former, standard method, considerable numerical difficulties were encountered in getting realistic simulations, while the latter methods experienced difficulties accurately approximating the target (P-M) spectrum, and an accurate approximation could only be feasible when using a high order AR scheme, (ibid). Spanos used dimensionless coefficients in his version of the ARMA model in order to utilize the filter for multiple wind conditions and sea states.

It was found that the spectrum of the time series generated by the AR model exhibited considerable narrowband fluctuations with respect to the P-M target spectrum. The fluctuations are thought to be associated with pole locations of the transfer function with respect to the unit circle. The dimensionless coefficients used by Spanos resulted in high frequency models that fail to match the P-M spectrum. Additionally, the form of dimensionless coefficients did not properly illustrate the behavior of ocean waves under different sea state conditions, compared to the nominal one chosen for the normalization. As it turns out, the mathematical form of the P-M spectrum cannot be realized exactly in a linear filter transfer function.

#### **D. OBJECTIVE OF THESIS**

Even though the spectral analysis of ocean wave-induced motions have been studied over a period of recent years, problems and limitations continue to exist. These limitations have made it difficult to predict sea state conditions; and consequently have made the task of efficiently operating Autonomous Underwater Vehicles challenging.

For an Autonomous Underwater Vehicle (AUV) to operate in shallow water with adequate reliability, wave forces and their effects on the AUV should be modeled mathematically with an adequate degree of accuracy. A major component of the mathematical model of these loads/forces experienced by underwater vehicles involves

ocean wave kinematics, (Sarpkaya and Isaacson, 1981). In fact, over a period of years the Pierson-Moskowitz (P-M) spectrum has dominated the statistical description of ocean wave kinematics, (Pierson and Moskowitz, 1964). Thus, in analyzing the impact of these forces on underwater vehicles, it is worthwhile to generate a time record of values of wave kinematics that is compatible with the P-M spectrum. Traditionally this has been achieved by relying on the harmonic superposition method, (Hudspeth and Borgman, 1979, Shinozuka, 1972, Shinozuka and Wai, 1979), which can be cumbersome and costly in terms of computation time. Recently, with emphasis placed on improving the computational time, Spanos developed a procedure based on digital filtering techniques. His method involved the design of an autoregressive filter (AR) and autoregressive moving average (ARMA) filter that consisted a transfer function whose squared modulus was a close of the target P-M spectrum, (Spanos and Hansen 1981, Spanos 1983). His digital filtering technique demonstrated promise in computational efficiency, nevertheless, it proved to be a delicate task for spectral matching, (Spanos and Mignolet, 1986).

In this thesis, seaway dynamics will be modeled as a linear system with a random white noise input, where the linear system transfer function is approximately mapped to the P-M spectrum. Further, this work will use a digital filtering technique from two transfer functions to approximate the P-M spectrum. Initially, the effectiveness of Spanos' AR and ARMA methods will be determined by testing the stability through eigenvalue analysis. These eigenvalues are to be modified as necessary to achieve required stability. This model will then be compared to the output of a digital filter generated from the transfer function of an eighth-order system. Once the results of the eighth-order system are compared to the results of the Spanos model for best mapping of the P-M and pressure profile spectra, at specified water depths, the system (eighth-order or Spanos) with the most accurate approximation of the P-M target spectrum will be further studied in a filter system and used to predict sea states and pressure responses at future times based on current and previous measurements. The accuracy will be measured using cross-correlation between the target spectrum and the dynamic equation/innovator.

## II. LINEAR PREDICTION THEORY (LPT)

### A. HISTORY AND FORMULATION OF LPT

Digital representation of sea surface elevation and pressure profile processes is called a time series. The probabilistic description of ocean and wave induced responses was introduced during the 1950s, (Spanos and Mignolet, 1986). Prior to the introduction of the Linear Prediction Theory (LPT), the traditional techniques for generation of simulated digital sea wave height, velocity, and acceleration records were based primarily upon the principle of wave superposition. For each point in time domain, this technique generally required the computation of a sum of harmonic waves, (Spanos and Hansen, 1981). Nevertheless, because of successful research efforts in the areas of simulation and processing of digital data in the time domain, modeling of sea wave time history with the Linear Prediction Theory has proven to be quite accurate. The LPT method provides an efficient procedure of generating a collection of records possessing a power spectrum which approximates a known target spectrum, (ibid). In the LPT, the records of sea waves are approximately compatible with the Pierson-Moskowitz (P-M) target spectrum, and are obtained as the output of a recursive digital filter with a random white noise input. The problem of base period repetition of wave records is thus avoided. Essentially, this technique simply realizes the approximation of the Pierson-Moskowitz (P-M) spectrum as the output of a digital filter to white noise excitation. More details on the development of the P-M Spectrum formulation will be addressed later.

When modeling the spectrum, the velocities and acceleration particles for sea wave simulations can be simulated utilizing the Linear Prediction Theory and the following relationships for the horizontal velocity  $P_v(\omega)$  and acceleration  $P_a(\omega)$  spectra, (Shinozuka, 1972)

$$P_v(\omega) = \omega^2 [G(\omega, z, H)]^2 P(\omega)$$

and

$$P_a(\omega) = \omega^4 [G(\omega, z, H)]^2 P(\omega)$$

where  $P(\omega)$  is the surface elevation spectrum, and  $G(\omega, z, H)$  is a function of  $\omega$  depending as well upon the total water depth ( $H$ ) and the vertical position ( $z$ ) above the sea floor where the velocity and acceleration simulations are desired. The independent variable  $\omega$  represents frequency in radians per second. Using  $P_v(\omega)$  and  $P_a(\omega)$  as target spectra, LPT can be applied to obtain time domain velocity and acceleration records. This method of simulation is based on an all-pole recursive filter, the input, as stated above, of which is a random white noise process. A one-time computation of the digital filter difference equation coefficients are required. Once these coefficients are computed for a particular target spectrum, they can be stored for future usage as necessary. The generation of the output time domain record requires only simulation of white noise digital samples and application of the difference equation. No computations of any trigonometric or other functions are required after the initial coefficient generation.

The LPT was utilized to digitally simulate the time domain sea wave height records. The target P-M spectrum was treated as one-sided extending over the frequency range  $(0, \omega_b)$ . White noise records were numerically simulated and used as input to the difference equation representing the digital filter. The difference equations and methods for determining the difference equation coefficients can be cited in (Spanos and Hansen, 1981). The Fast Fourier Transform (FFT) of the digital time record generated by the difference equation was used to calculate the response spectrum of the digital filter output.

The following figures represent the results obtained using LPT. Figure 1 illustrates an example record for an upper frequency  $\omega_b = \pi/2$  rad/sec, filter of order  $p = 25$ , and wind velocity of 40 knots. Figure 2 illustrates a portion of a record which is the output of a digital filter of order 50, upper frequency of  $\omega_b = \pi/2$  rad/sec, and wind velocity of 40 knots. Figure 3 is the average power spectrum of 300 records of 1000 time

increments length for an upper frequency  $\omega_b = \pi/2$  rad/sec and wind velocity of 40 knots. A sampling interval of  $T = 2$  seconds between pulses of the filter output to white noise input was used. This procedure was repeated for simulations of lower order filters as well. Noticeably, a trend of decreased mapping between the P-M target spectrum and power spectrum waves of the filter output was obvious. Figures 4 through 7 illustrate records and power spectra of outputs of filters of orders 25 and 40 respectively, with frequency  $\omega_b = \pi/3$  rad/sec, a sampling interval of  $T = 3$  seconds, and a wind velocity of 40 knots.

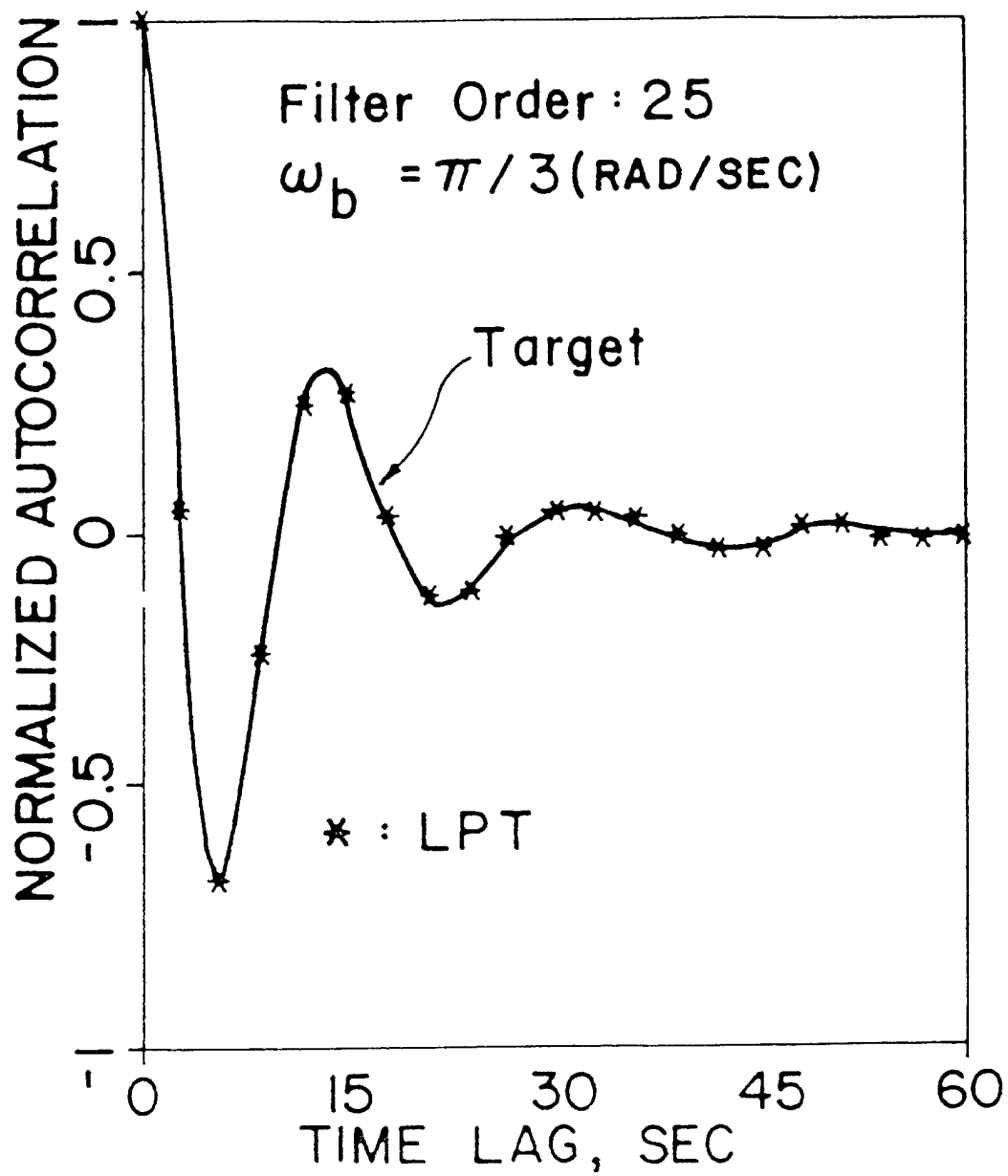


Figure 1. Normalized autocorrelation, (Spanos and Hansen, 1981).

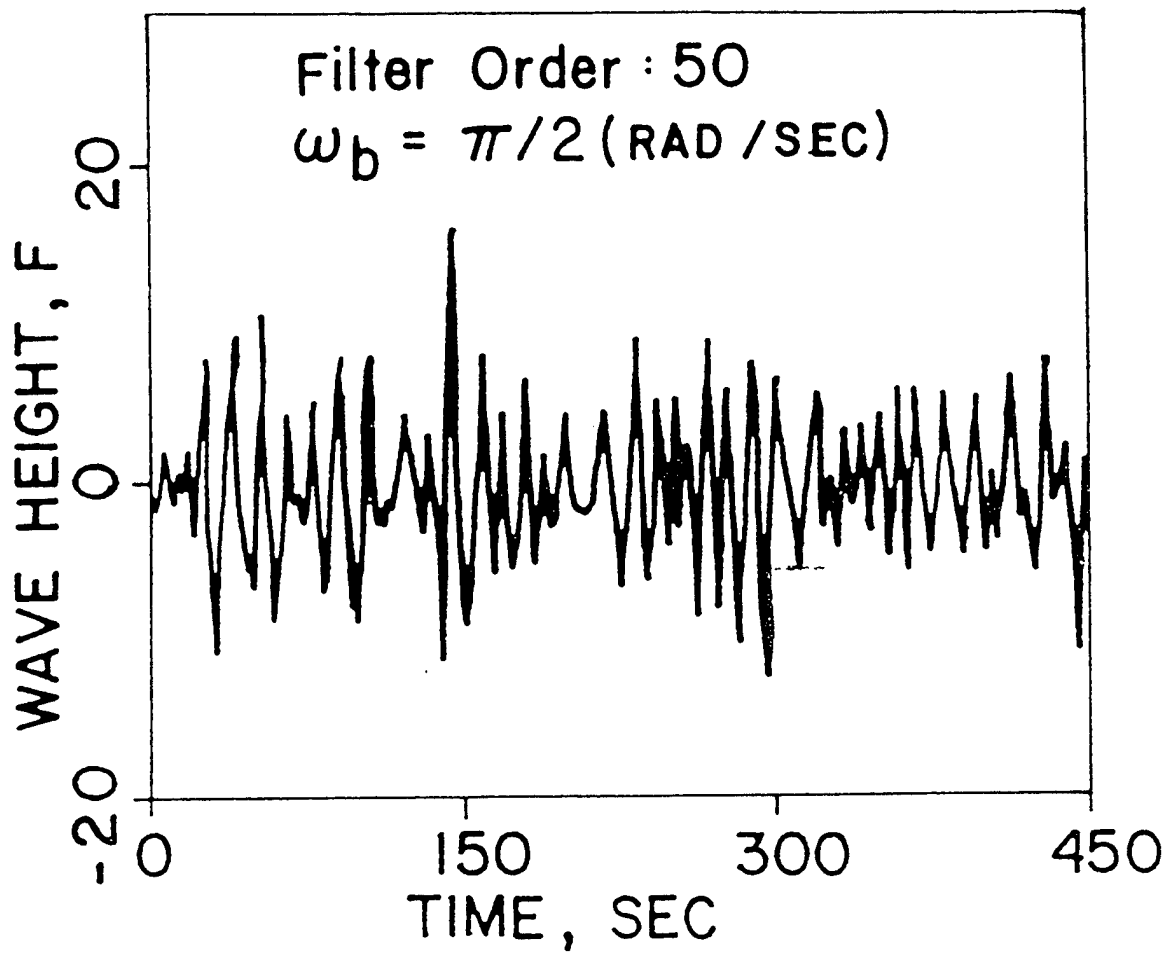


Figure 2. Portion of a LPT-simulated sea wave height record,  
(Spanos and Hansen, 1981).

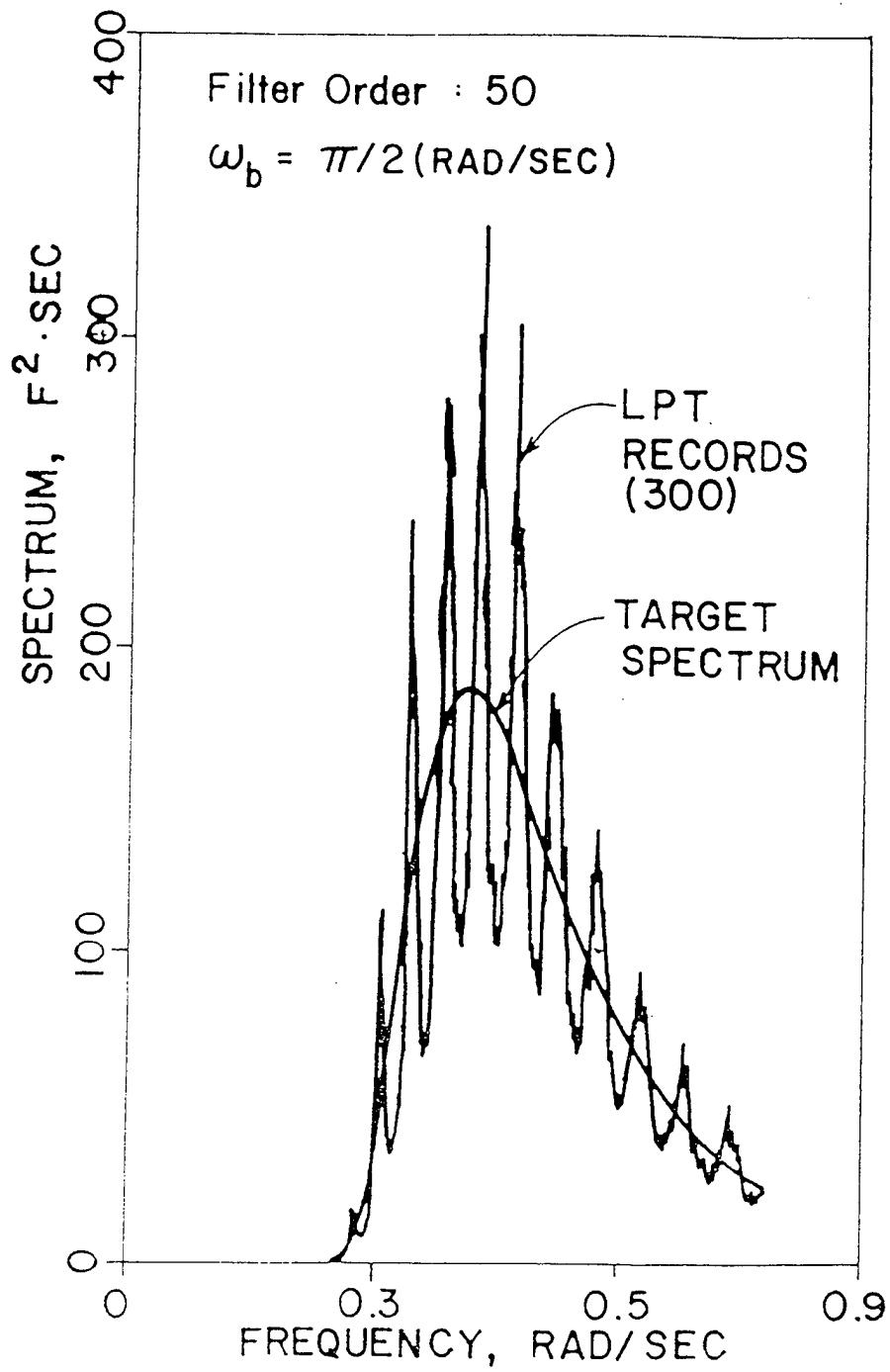


Figure 3. Average Fast Fourier Transform (FFT) of 300 LPT-simulated sea wave height records, (Spanos and Hansen, 1981).

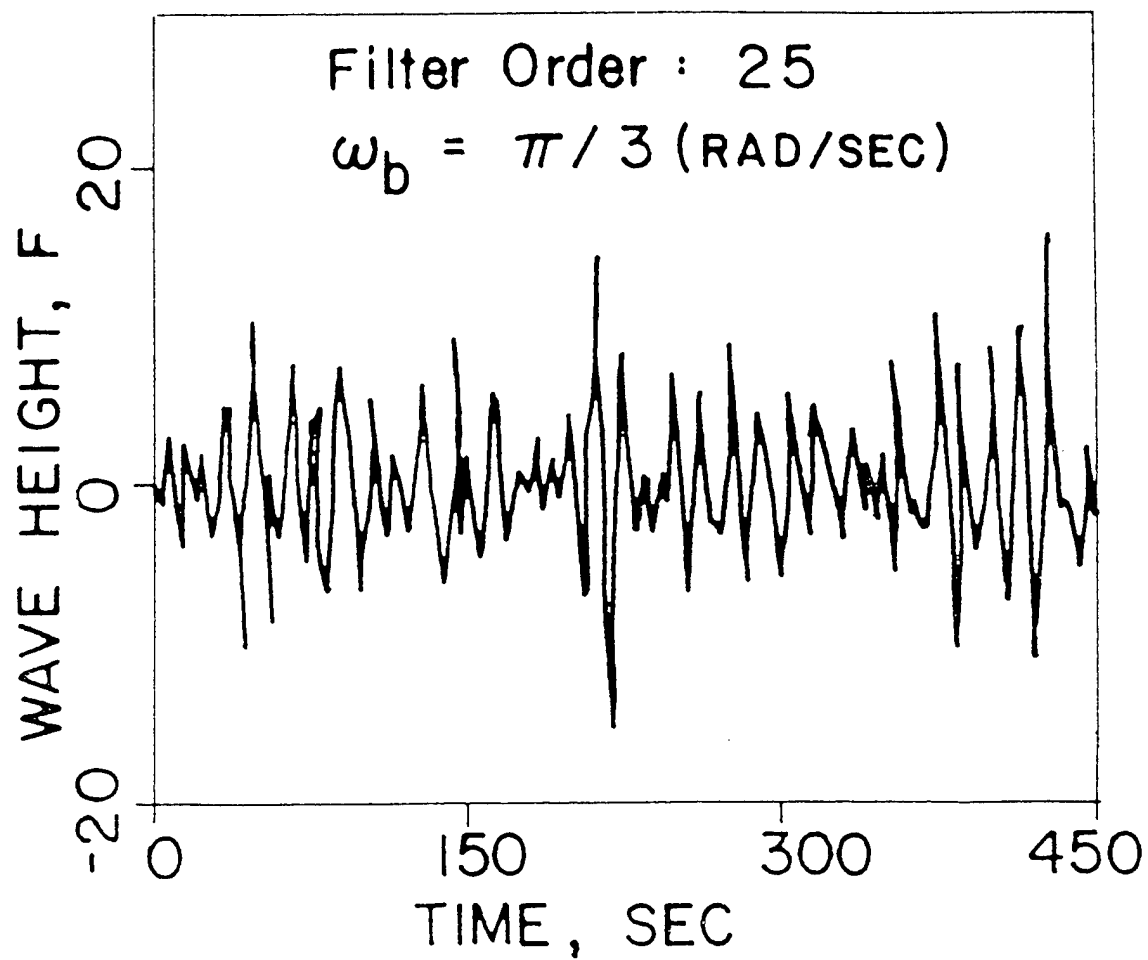


Figure 4. Portions of a LPT-simulated sea wave height record, (Spanos and Hansen, 1981).

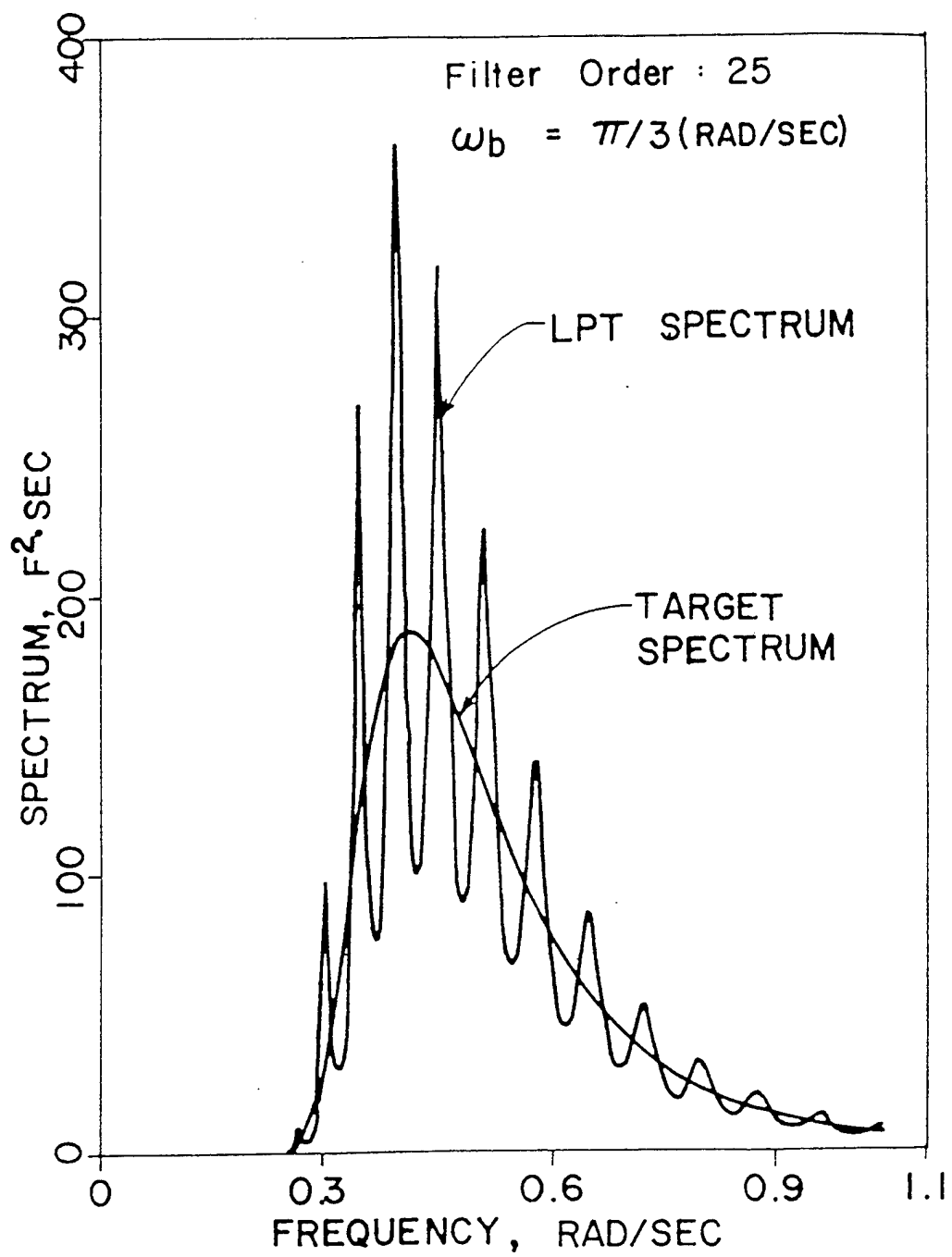


Figure 5. Power Spectrum of LPT-simulated sea wave height record, (Spanos and Hansen, 1981).

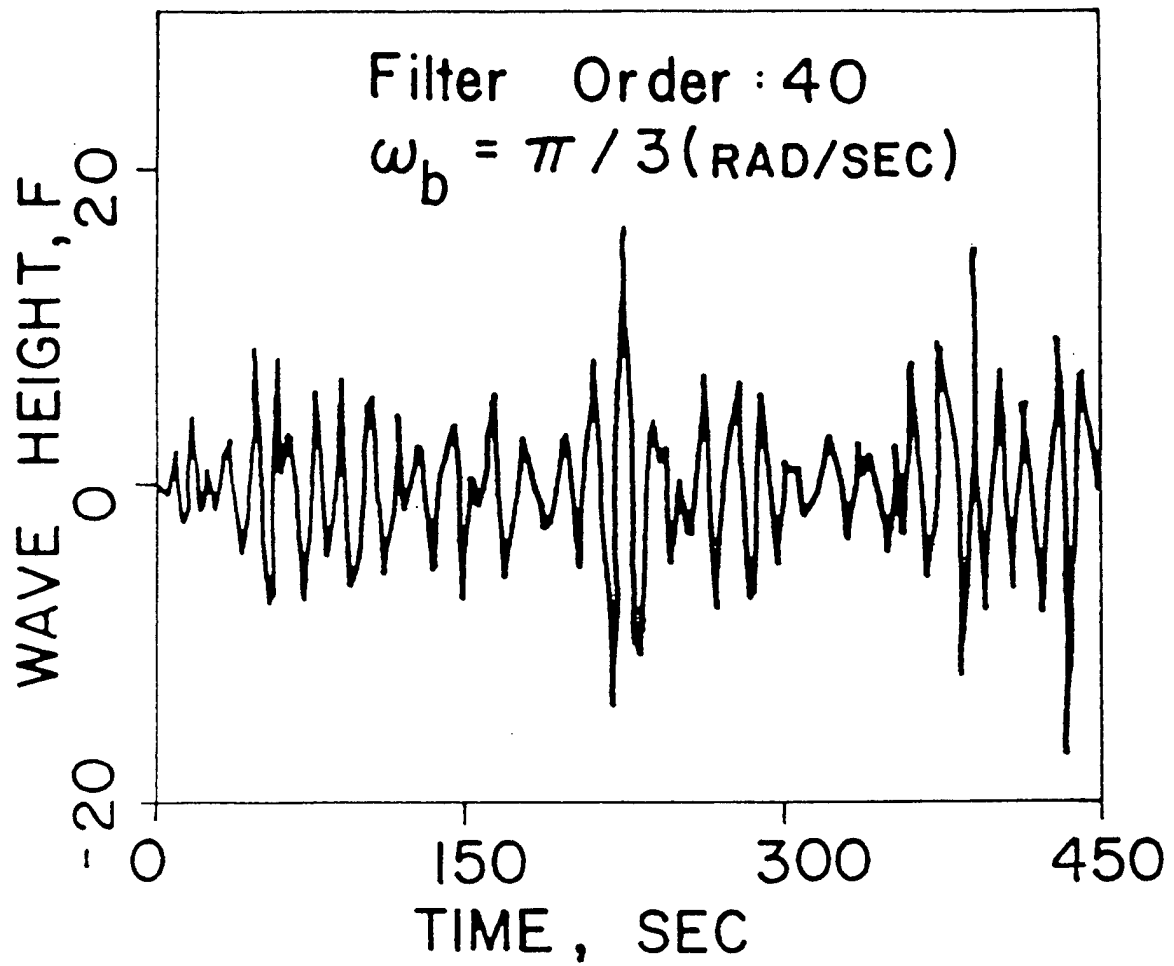


Figure 6. Portions of a LPT-simulated sea wave height record, (Spanos and Hansen, 1981).

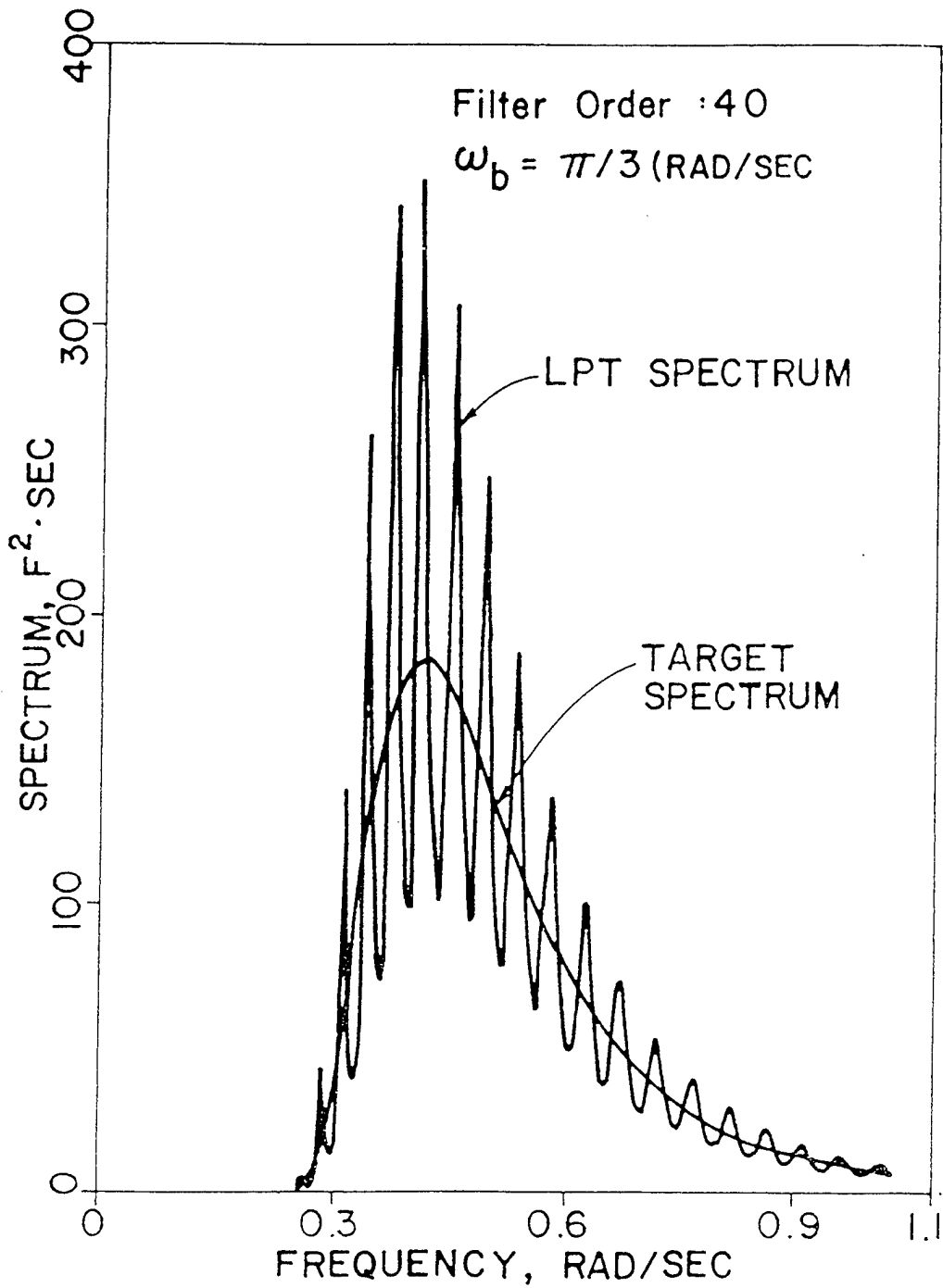


Figure 7. Power spectrum of LPT-simulated sea wave height record, (Spanos and Hansen, 1981).

## B. MODELING OF THE SYSTEM AND REAL TIME-FORWARD PREDICTION

The general block diagram model of the proposed overall system including the target spectrum transfer and the transfer function of the dynamic equation/filter with the innovator gains illustrated is depicted below in Figure 8.

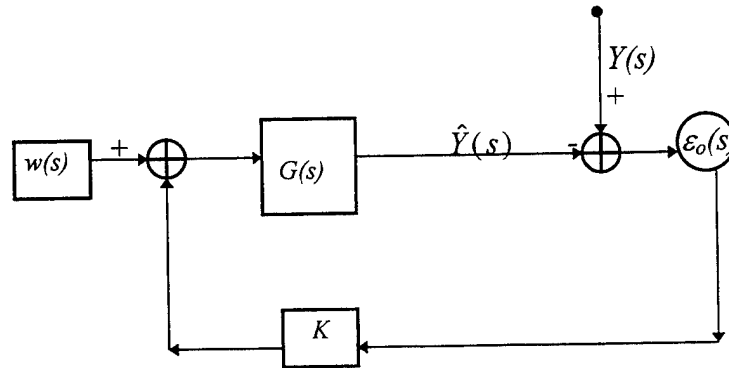


Figure 8. Block diagram of system

where  $w(s)$  is the white noise input,  $\hat{Y}(s)$  is the filtered estimate of the under wave pressure response,  $Y(s)$  is the measured pressure,  $\epsilon_o(s)$  is the error between  $Y(s)$  and  $\hat{Y}(s)$ , and  $K$ 's are the system gains. The independent variable  $s$  represents the Laplace variable.

If the following expression is stable then the error ( $\epsilon$ ) between the filter estimate and the wave response is a bounded value as  $t \rightarrow \infty$ .

$$\frac{G(s)}{1 + KG(s)}$$

$Y(s)$ , wave motion (i.e. measured pressure signal) is assumed to arise from a random white noise driven system with a dynamic transfer function where,

$$\|G(\omega)\|^2 = S(\omega)$$

Spanos developed a transfer function (in terms of  $z$ -transformation) which is a simple version of the more general higher order general Autoregressive Moving Average (ARMA) model.

$$G(z) = \frac{X}{U} = \frac{\sum_{j=0}^m b_j z^{-j}}{1 + \sum_{k=1}^l a_k z^{-k}}$$

This transfer function in terms of  $z$ -transformation notation was used as the output of the digital filter which is represented by the symbol  $Y(t)$ .

In Spanos' dimensionless model the coefficients  $a_i$  and  $b_i$  were optimally chosen to minimize error between the Pierson Moskowitz target spectrum equation and the transfer function of the ARMA filter. Spanos presented the coefficients in dimensionless forms in order to use them in various structural dynamic applications. Nevertheless, when attempting to model a dynamic equation for the target P-M spectrum, the transfer function generated by the coefficients of the dimensionless model resulted in a narrow band, high frequency spectrum that failed to adequately resemble and map the P-M spectrum. The high frequency results are illustrated in Figure 9. Additional problems were encountered with normalization - it was difficult to reconstitute and stabilize the system, and the transfer function had unstable zeros, more details on Spanos' ARMA in following chapters.

Mathematical calculations determining the error between the P-M target spectrum (wave and pressure responses) and the dynamic equation/filter have been performed to verify the validity of the system's block diagram. Figure 10 illustrates a modified block diagram of the system which emphasizes how the error ( $\varepsilon$ ) is measured schematically. Assuming that the seaway can be represented as the output from a white noise driven filter, generally, the error ( $\varepsilon$ ) goes to zero when the wave and pressure responses  $G(s)$  equals or matches the response of the dynamic equation  $S(\omega)$ , or simply :

$$\varepsilon \rightarrow 0; \|G(\omega)\|^2 \equiv S(\omega)$$

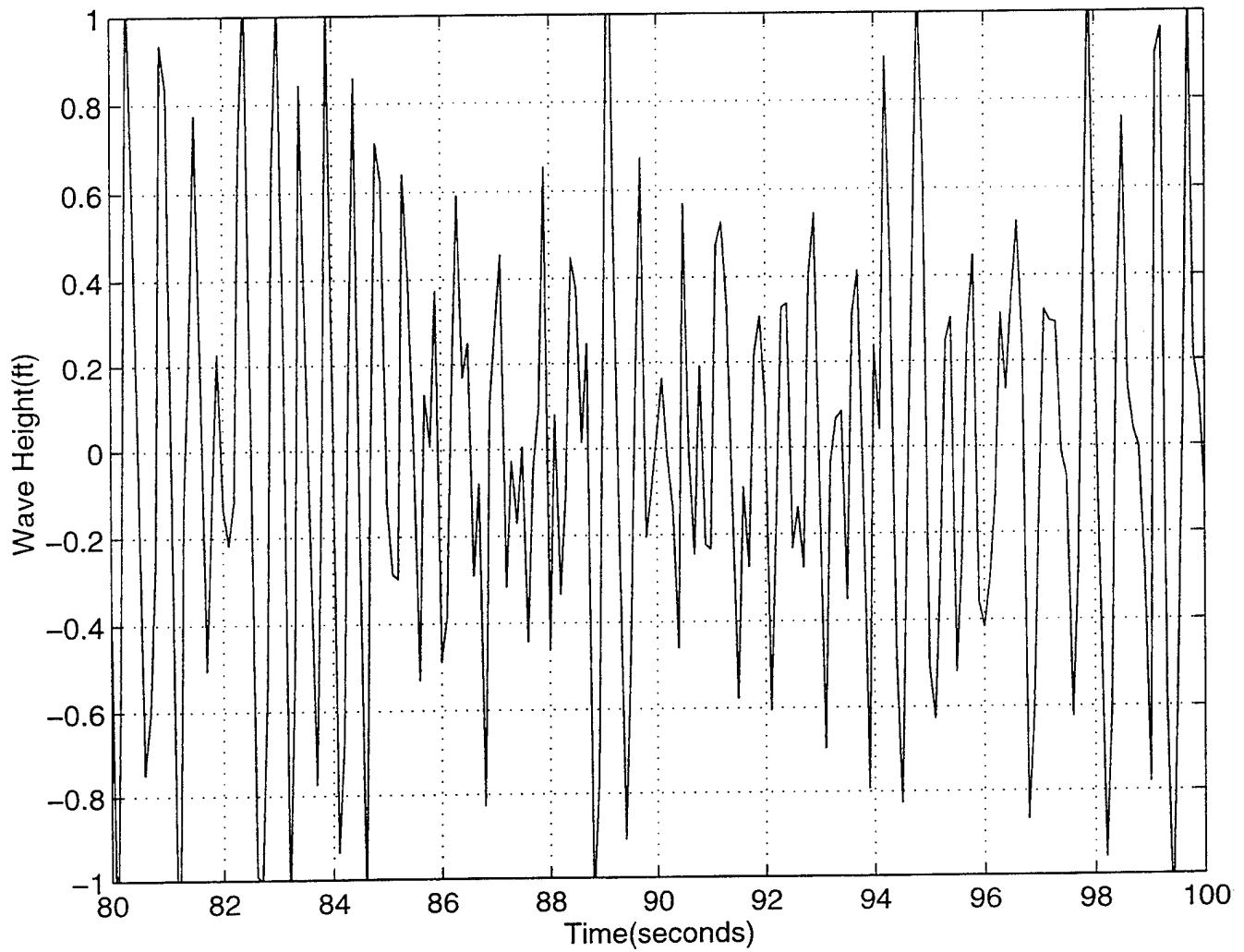


Figure 9. Time Record of Spanos' Dimensionless ARMA Model

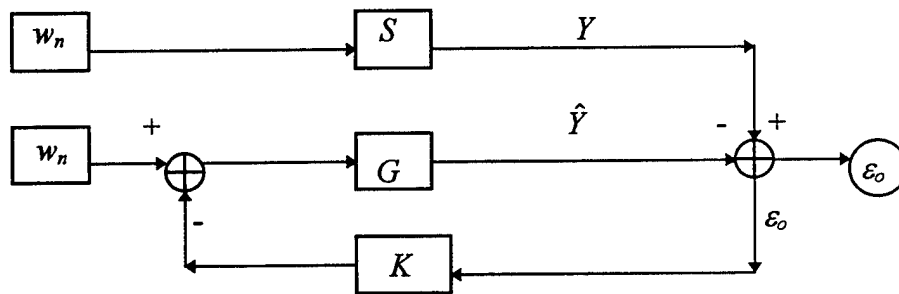


Figure 10. Block diagram of Forward Prediction System, where  $s$  = seaway internal dynamics and  $P_{PM} = \|S\|^2$

Assuming, for the moment that all white noise inputs are unity,

$$\varepsilon = \hat{Y} - Y = -S * w + G(w - K\varepsilon)$$

therefore,

$$\varepsilon(1 + GK) = (G - S)w \Rightarrow \varepsilon = \frac{(G - S)}{(1 + GK)}w$$

From examining the numerator of the above expression, it is obvious that when  $G=S$  the numerator is zero, therefore  $\varepsilon=0$ , and if  $GK$  is stable,  $\varepsilon$  is bounded and depends on

$$\|G - S\| \leq \|G\| - \|S\|$$

since  $G$  and  $S$  are both positive, real.

The equation to follow is given in terms of a transfer function, and has been used to mathematically model the transfer function of the dynamic system. In the work of Spanos, the equation is given as the digital filter of the following transfer function represented in terms of  $z$ -transformation:

$$G(z) = \frac{\sum_{j=0}^m b_{jk} z^{-k}}{1 + \sum_{k=1}^l a_k z^{-k}}$$

In this domain,  $z$  is the complex variable  $z = e^{Ts}$ , and  $s$  is the continuous time Laplace variable. For frequency inputs,  $s = j\omega$  ( $\omega$  is the radian frequency), in terms of the

corresponding frequency response of the discrete time system, we substitute  $z = e^{j\omega T}$ , and the magnitude of the system transfer function becomes

$$|G| = \frac{\left\| \sum_{j=0}^m b_{jk} e^{-j\omega k T} \right\|}{\left\| 1 + \sum_{k=1}^l a_k e^{-j\omega k T} \right\|}$$

which depends on both,  $\omega$  and  $T$ .

For Time Domain Representation:

Take  $G$  from the model and convert it to the following equation in the continuous time domain.

$$\dot{x}(t) = Ax(t) + Bu(t), y = Cx$$

where  $0 < t < \infty$ , and  $x(t)$  is a continuous state and  $u(t)$  is a continuous input of the interval  $0 < t < \infty$ , with the initial values  $x(t = 0)$ ,  $u(t = 0)$  and  $u(t > 0)$  being a series of zero order hold data such that at  $t_k = kdt$ ,  $u(t_k)$  is a data sequence: Between the intervals  $t_k < t < t_{k+1}$ , where  $u(t) = u_b$  (Figure 11).

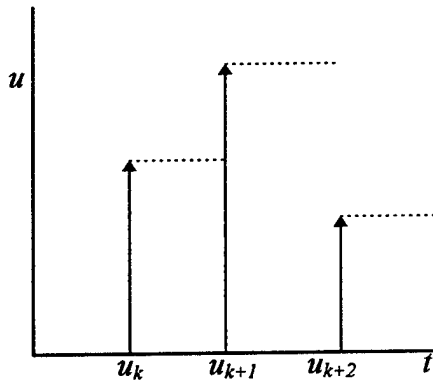


Figure 11. Represents Discrete Time Domain

The solution for  $x(t=t_k)$  is given by the following integral

$$\int_{t_k}^{t_{k+1}} \dot{x}(t) dt = \int_{t_k}^{t_{k+1}} Ax(t) dt + \int_{t_k}^{t_{k+1}} Bu(t) dt$$

giving

$$x_{k+1} = (e^{aT})x_k + (e^{aT} - 1)a^{-1}bu_k \Rightarrow x_{k+1} = \phi x_k + \gamma u_k$$

where

$$\phi = e^{aT} \text{ and } \gamma = (e^{aT} - 1)A^{-1}B.$$

This converts  $\dot{x} = Ax + Bu$  to the following system in discrete sampled time domain

$$x(t) = \Phi x(t-1) + \Gamma u(t)$$

$$y(t-1) = Cx(t-1)$$

Initially, Spanos used pole placement to design the control matrix,  $K$ . However, the Linear Quadratic Regulator (LQR) proved to be more convenient for determining the values of the gain matrix, leading to the estimator ( $u$  in this case is zero mean, white noise)

$$\hat{x}_{k+1} = \Phi \hat{x}_k + K(p_k - \hat{p}); \quad \hat{p} = C\hat{x}_k$$

where  $p_k$  is defined as the measured pressure from the Pierson-Moskowitz and pressure profile spectrum.

Simplifying the above equation yields:

$$\hat{x}_{k+1} = (\Phi - KC)\hat{x}_k + Kp_k; \quad \hat{p}_k = C\hat{x}_k$$

The best estimate/prediction forward in time is then using the above model without data correction obtained through the following equation from the discrete time domain. This forward prediction is always based on the estimated quantity of  $\hat{x}(t)$  :

$$\hat{p}(t+k) = \Phi^k C\hat{x}(t)$$

### C. PROBLEMS ENCOUNTERED WHEN USING LINEAR PREDICTION THEORY (LPT)

This method superseded the harmonic superposition method. However, it proved to be quite cumbersome for data processing machines requiring immense computational time. Problems were noted with the fluctuation of the LPT-generated spectrum from the target spectrum. Figures 3,5 and 7 illustrate these fluctuations. The LPT is not always computational efficient for simultaneous simulation of sea wave velocity and acceleration records at several times, and points with any combination of horizontal and vertical coordinates, (Spanos and Hansen, 1981). Considering the behavior of the power spectra when mapping it with the target spectrum as the order of the filter  $p$  was decreased, it was discovered that increasing the filter order  $p$ , the local frequency breadth of the spectral fluctuation decreases, (ibid).

Using an approximation of the P-M spectrum as the output of digital filters to white noise excitation has been proven to have numerical difficulties when approximating it by the Autoregressive (AR) models, (Spanos, 1983). However, when using the AR model as an initial spectral approximation, it proves to yield an efficient autoregressive moving average (ARMA) model, (Spanos and Mignolet, 1986).

### III. APPLICATION TO WAVE MOTION PREDICTION

#### A. PIERSON-MOSKOWITZ (P-M) SPECTRUM

A semi-empirical expression for the frequency spectrum of fully developed seas is given by,

$$S(\omega) = \frac{\alpha g^2}{\omega^5} \exp \left[ \beta \left( \frac{g}{V\omega} \right)^4 \right]$$

This expression was proposed by Pierson and Moskowitz for the height of fully developed seas, (Pierson and Moskowitz, 1964). The  $\alpha$  and  $\beta$  coefficients are nondimensional parameters defining the spectrum. The P-M spectrum was developed for wind velocity at a standard height of 19.5 meters above the free surface. This two parameter spectrum is sufficiently general to fit quite a few observations and is consistent with theoretical predictions of the high frequency limit. Where most common values for the nondimensional parameters are

$$\alpha = 8.1 \times 10^{-3}$$

$$\beta = -0.74$$

The gravity constant is

$$g = 32.174 \text{ ft/sec}^2$$

The two variables in the expression are

$$\omega = \text{frequency (rad/sec)}$$

$$V = \text{wind speed (ft/sec)}$$

The Pierson and Moskowitz expression can be further reduced by considering the relationship between the significant wave height,  $H_{1/3}$ , and wind speed,  $V$ . The following expression represents the aforementioned relationship:

$$H_{1/3} = 4.0 \left( \int_0^{\infty} S(\omega) d\omega \right)^{1/2} = 0.2092 \frac{V^2}{g}$$

Substituting this relation, along with the specified nondimensional parameters and gravity constant, into the Pierson and Moskowitz spectra equation yields a simplified version of the P-M expression which was used to generate the P-M and pressure profiles for the target spectrum ( $S(\omega)$ ). The simplified expression is

$$S(\omega) = \frac{8.1 \times 10^{-3} \times 32.174^2}{\omega^5} \times \exp \left[ -0.74 \left( \frac{32.174^2 \times 0.2092^2}{H^2 \times \omega^4} \right) \right]$$

where  $H$  was for (the mean water depth) shallow water, linear waves for this particular model is 7 meters (approximately 23 feet). (Papoulias, 1993)

Typical plots of varying significant wave heights ( $H_s$ ) versus frequency and period for P-M spectra are illustrated in Figures 12 and 13 respectively.

## B. PIERSON-MOSKOWITZ (P-M) AND PRESSURE PROFILE TARGET SPECTRUM

In performing digital time series analysis, the sampling period  $T$  and the cut-off frequency  $\omega$ , are related through the Nyquist relation  $T = \pi/\omega$ . In order to generate the appropriate target spectrum at a specified operating depth, in this case 5.2 meters (approximately 17 feet) below the surface, the pressure at this depth had to be considered. To this end, the P-M expression was multiplied by  $G(\omega, z, H)$  which resulted from the linear wave theory. Plots consisting of varying significant wave heights ( $H_s$ ) versus frequency and period for P-M and pressure profile spectra are illustrated in Figures 14 and 15 respectively.

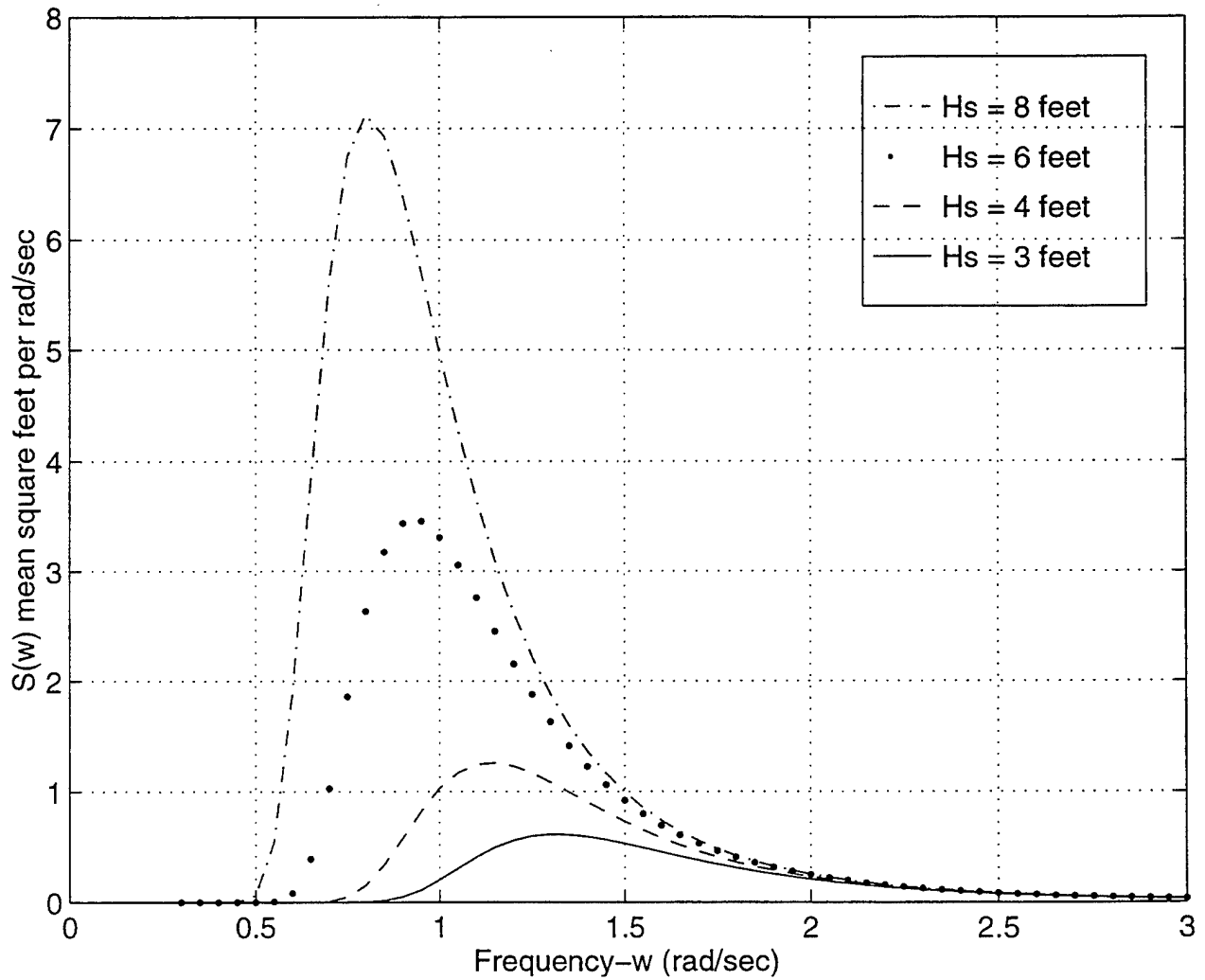


Figure 12. Pierson-Moskowitz (P-M) spectra for significant height ( $H_s$ ) of 8, 6, 4, and 3 feet versus frequency.

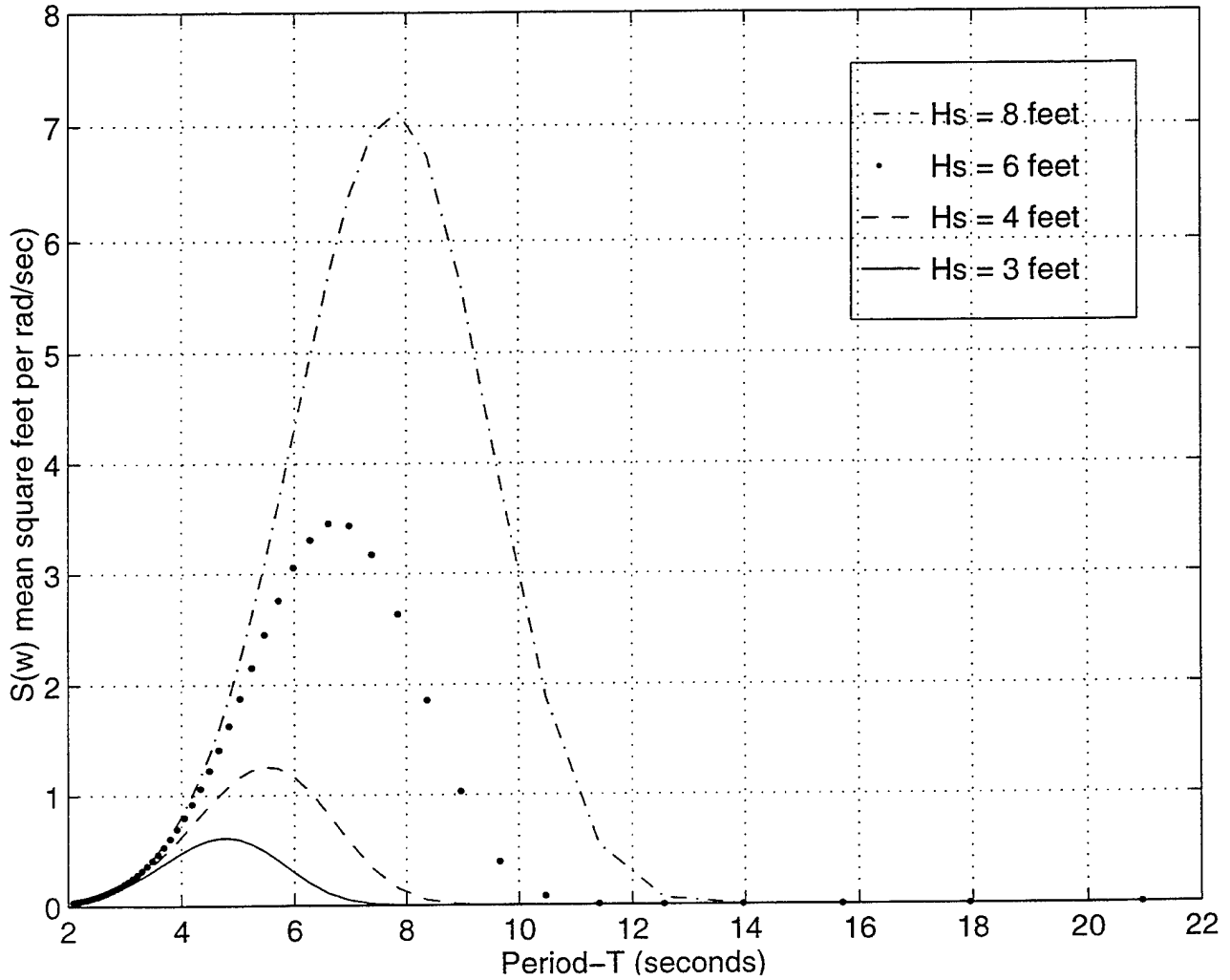


Figure 13. Pierson-Moskowitz (P-M) spectra for significant height ( $H_s$ ) of 8, 6, 4, and 3 feet versus periods.

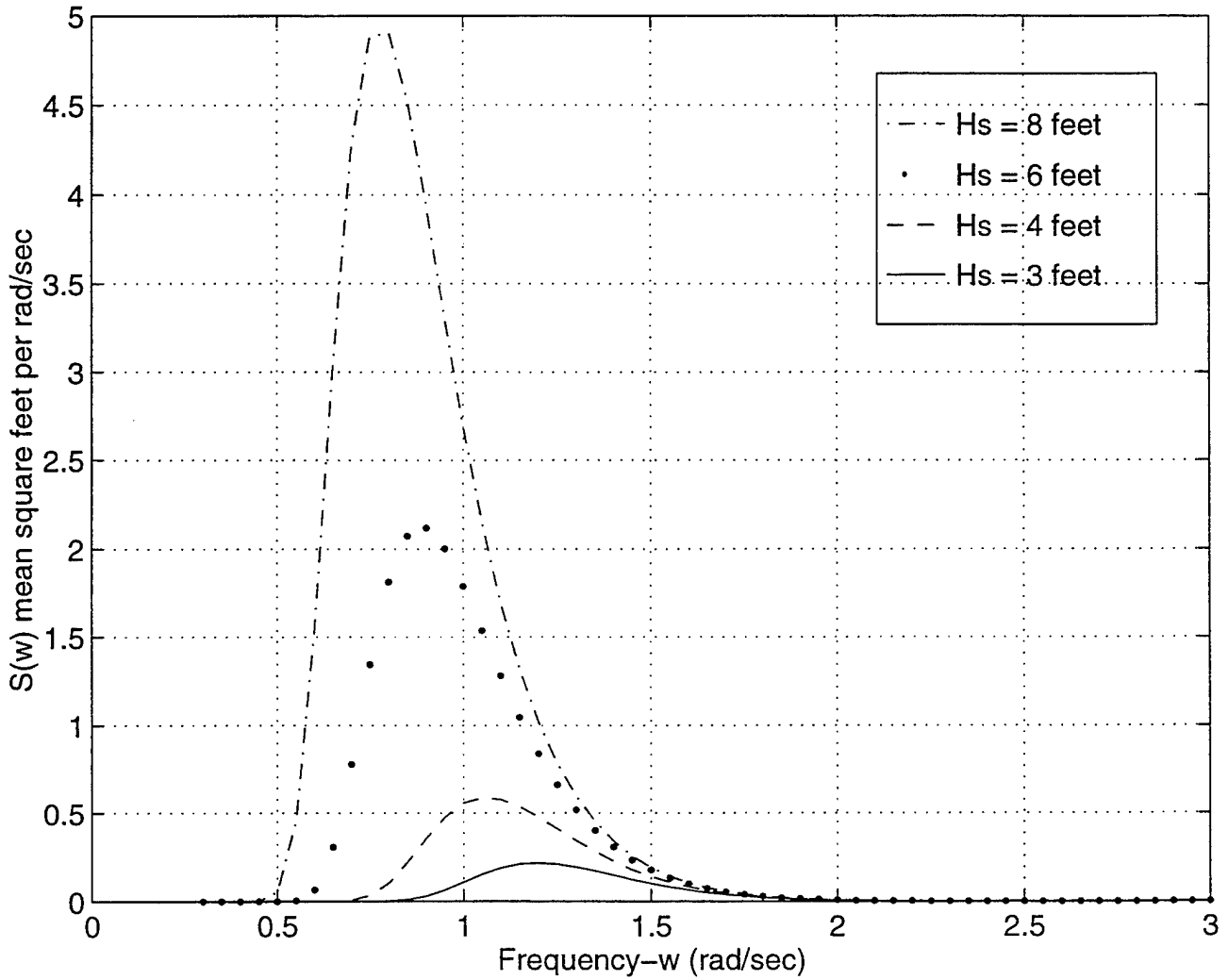


Figure 14. Pierson-Moskowitz (P-M) and pressure profile spectra for significant height ( $H_s$ ) of 8, 6, 4, and 3 feet versus frequency.

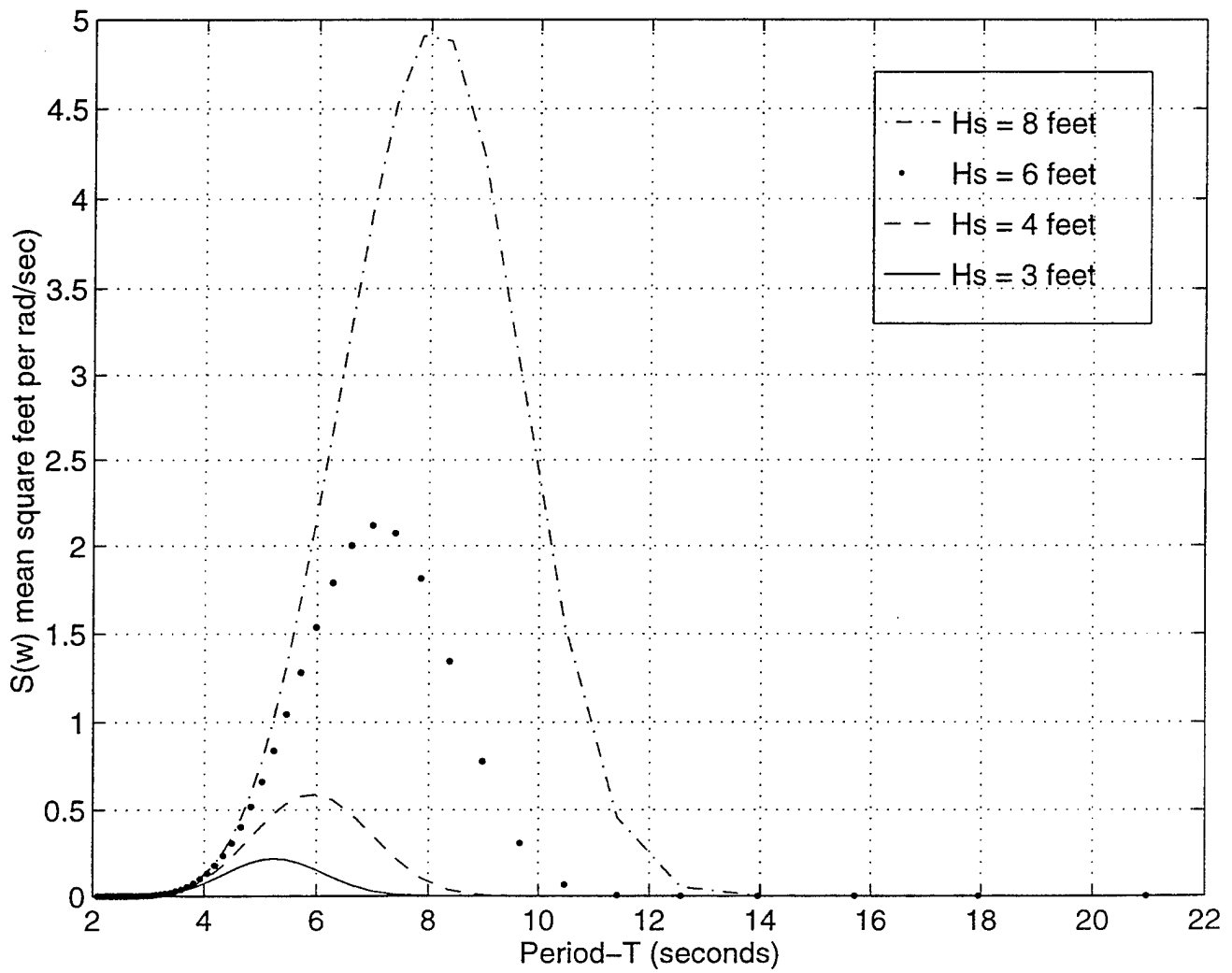


Figure 15. Pierson-Moskowitz (P-M) and pressure profile spectra for significant height ( $H_s$ ) of 8, 6, 4, and 3 feet versus periods.

The Depth Modifier for pressure variation expression is

$$P_{\text{wave}}(t,x,z) = \rho g z + \eta_a \rho g \left[ \frac{\cosh(2\Pi(H-z)/\lambda)}{\cosh(2\Pi H/\lambda)} \right] \sin \left[ 2\Pi \left( \frac{t}{T} - \frac{x}{\lambda} \right) \right]$$

Revised Depth Modifier for the pressure variation expression neglecting gravity

$$G(z,H,\lambda) = \left[ \frac{\cosh(2\Pi(H-z)/\lambda)}{\cosh(2\Pi H/\lambda)} \right]$$

The expression for generating P-M and pressure profile target spectrum is

$$\frac{8.1 \times 10^{-3} \times 32.174^2}{\omega^5} \times \exp \left[ -0.74 \left( \frac{32.174^2 \times 0.2092^2}{H^2 \times \omega^4} \right) \right] \times \left[ \frac{\cosh(2\Pi(H-z)/\lambda)}{\cosh(2\Pi H/\lambda)} \right]$$

Taking the **regular wave theory**, and assuming a horizontal sea bottom and a free-surface of infinite horizontal extent, a linear wave theory for propagating waves can be derived. This derivation applies the free-surface and sea bottom conditions, (Faltinsen, 1990), and the Laplace equation  $\nabla^2 \phi = 0$ . The mean water depth will be defined by the constant  $H$ . The following expression then gives the connection between wavelength  $\lambda$  and wave period  $T$  for a finite water depth.

$$\lambda = \frac{g}{2\pi} T^2 \tanh \frac{2\pi}{\lambda} H$$

Substituting  $\omega = 2\pi/\lambda$  in the above expression and simplifying the nonlinear quadratic equation yields

$$f = \left[ \lambda \left( \frac{(\omega)^2}{2\Pi} \right) - g \tanh\left(2\Pi H / \lambda\right) \right] = 0$$

where all values of lambda  $\lambda$  were found as functions of frequency  $\omega$ , for this particular depth condition see Table 1.

For this particular research, the wavelength and frequency connection equation was solved for a specified mean water depth ( $H$ ) of 7 meters. The quadratic was solved using the recurrence equation solver in conjunction with the floating-point arithmetic solver from the Maple Software Application. The frequency range for lambda  $\lambda$  as a function of  $\omega$  is  $0.2 < \omega(i) < 3$ , in increments of 0.05.

Thorough details regarding the derivation of linear wave theory for propagating waves are beyond the scope of this work, however, information can be found in many textbooks in fluid mechanics (for instance Newman, 1977, chapter 6), (Faltinsen, 1990). The equations for free-surface and sea bottom conditions, along with the relations of wavelength  $\lambda$  and period  $T$  can be cited in (Faltinsen, 1990).

$\omega$ (rad/sec)	$\lambda$ (meters)	$\omega$ (rad/sec)	$\lambda$ (meters)	$\omega$ (rad/sec)	$\lambda$ (meters)
0.3	171.61	1.05	43.05	2.05	14.59
0.35	146.52	1.1	40.49	2.1	13.92
0.4	127.62	1.15	38.14	2.15	13.29
0.45	112.86	1.2	35.96	2.2	12.70
0.5	100.98	1.25	33.93	2.25	12.15
0.55	91.21	1.3	32.05	2.3	11.63
0.6	83.01	1.35	30.29	2.35	11.15
0.65	76.02	1.4	28.64	2.4	10.69
0.7	70	1.45	27.10	2.45	10.26
0.75	64.73	1.5	25.66	2.5	9.86
0.8	60.08	1.55	24.30	2.55	9.47
0.85	55.94	1.6	23.03	2.6	9.11
0.9	52.23	1.65	21.84	2.65	8.77
0.95	48.88	1.7	20.71	2.7	8.45
1.0	45.83	1.75	19.66	2.75	8.15
-	-	1.8	18.67	2.8	7.86
-	-	1.85	17.75	2.85	7.59
-	-	1.9	16.88	2.9	7.33
-	-	1.95	16.07	2.95	7.08
-	-	2.0	15.30	3.0	6.85

Table 1. Lambda ( $\lambda$ ) defined as function of omega ( $\omega$ ) for water depth of  $H = 7$  meters (approximately 23 feet).

### C. SPANOS' DIMENSIONLESS ARMA FILTER

Recently, Spanos developed a digital filtering techniques that involved the design of an autoregressive moving average (ARMA) filter having a transfer function whose squared modulus was assumed to be a close approximation of the target P-M spectrum. The transfer function of the ARMA( $l, m$ ) process  $y$  is a discrete random process whose  $n^{\text{th}}$  sample can be obtained from the previous one using the following expression:

$$y_n = -\sum_{k=1}^l a_k y_{n-k} + \sum_{j=0}^m b_j \omega_{n-j}$$

where  $\omega$  denotes a bandlimited  $[-\omega_b, \omega_b]$  white noise process with autocorrelation function, (Spanos and Mignolet, 1986).

Spanos also used the process  $y$  as the output of a digital filter of a transfer function in the terms of z-transform notation. The input to this transfer is a discrete band limited white noise process  $\omega$ .

$$H(z) = \frac{\sum_{j=0}^m b_j z^{-j}}{1 + \sum_{k=1}^l a_k z^{-k}}$$

This transfer function was examined using the dimensionless coefficients in Table 2. After comparing the power spectrum of the transfer function and developing a wave record, it was discovered that this process resulted in a very high frequency record which was far from mimicking the behavior of ocean waves. This behavior was cited earlier in Figure 9. Consequently, another attempt to utilize this transfer function for matching the P-M Spectrum was made by modifying the numerator in order to best represent wave motions.

Manipulating the latter transfer function by taking the z transforms to get a z-domain (ARMA) model of system dynamics yields

$$zX = \phi X + \gamma U \Rightarrow (z - \phi)X = \gamma U$$

where  $\phi = e^{\Delta T} \in R^{m \times m}$  and  $\gamma \in R^{m \times 1}$

therefore,

$$G(z) = \frac{X}{U} = [zI - \phi]^{-1} \gamma \Rightarrow G(z) = \frac{\gamma z^{-1}}{I - \phi z^{-1}}$$

where  $\gamma$  and  $\phi$  are m and n<sup>th</sup>-order polynomial expressions.

Spanos ARMA model transfer function is simplified to a more general higher order ARMA model expression such as:

$$G(z) = \frac{\sum_{j=1}^m b_j z^{-j}}{1 + \sum_{k=1}^l a_k z^{-k}}$$

in which  $b_j$  and  $a_k$  are related to  $\gamma$  and  $\phi$ .

Number	Coefficient ( $b_i$ )	Coefficient ( $a_i$ )
0	$8.1047 \times 10^{-2}$	-
1	$-2.5140 \times 10^{-1}$	$-9.2280 \times 10^{-1}$
2	$1.1136 \times 10^{-1}$	$2.3080 \times 10^{-2}$
3	$3.7368 \times 10^{-1}$	1.3286
4	$-3.8057 \times 10^{-1}$	$-8.9433 \times 10^{-1}$
5	$-1.2058 \times 10^{-1}$	$2.1836 \times 10^{-1}$
6	$2.3579 \times 10^{-1}$	$3.4409 \times 10^{-1}$
7	$-8.5629 \times 10^{-3}$	$-1.9221 \times 10^{-1}$
8	$-4.1185 \times 10^{-2}$	$8.6611 \times 10^{-2}$

Table 2. Spanos' P-M Wave Elevation Spectrum ARMA Coefficients (dimensionless).

#### D. EIGHTH-ORDER FILTER

Taking into account Spanos used an eighth-order transfer function to generate the system of dimensionless coefficients, a eight-order filter was assumed to be best suited for generating a filter to model the target spectrum in this work. However, spectral densities or wave spectra for transfer functions of different orders, ranging from second to eight-order systems were evaluated and compared to the target wave spectrum. After evaluating the spectrum of all aforementioned ordered systems, the spectrum of the eighth-order system, as expected, most closely reflected that of the target wave spectrum. The comparison between the target wave spectrum and the eighth-order system's spectrum is depicted in Figure 16.

The following expression was used to formulate the eighth-order transfer function for the dynamic equation which was used as filter to forward predict seaway surface elevation.

$$\left[ \frac{s/\omega_o}{1 + 2\zeta\left(\frac{s}{\omega_o}\right) + \left(\frac{s}{\omega_o}\right)^2} \right]^4$$

Generally, the eighth-order filter process  $\hat{P}$  is a discrete random process whose  $k^{\text{th}}$  sample can be obtained from the previous sample  $k$  in the following way

$$x_{k+1} = \phi x_k + q; \hat{P}_k = Cx_k$$

where the state matrix  $\phi$  is determined by the transfer function and  $q$  is a random white noise input with zero mean.

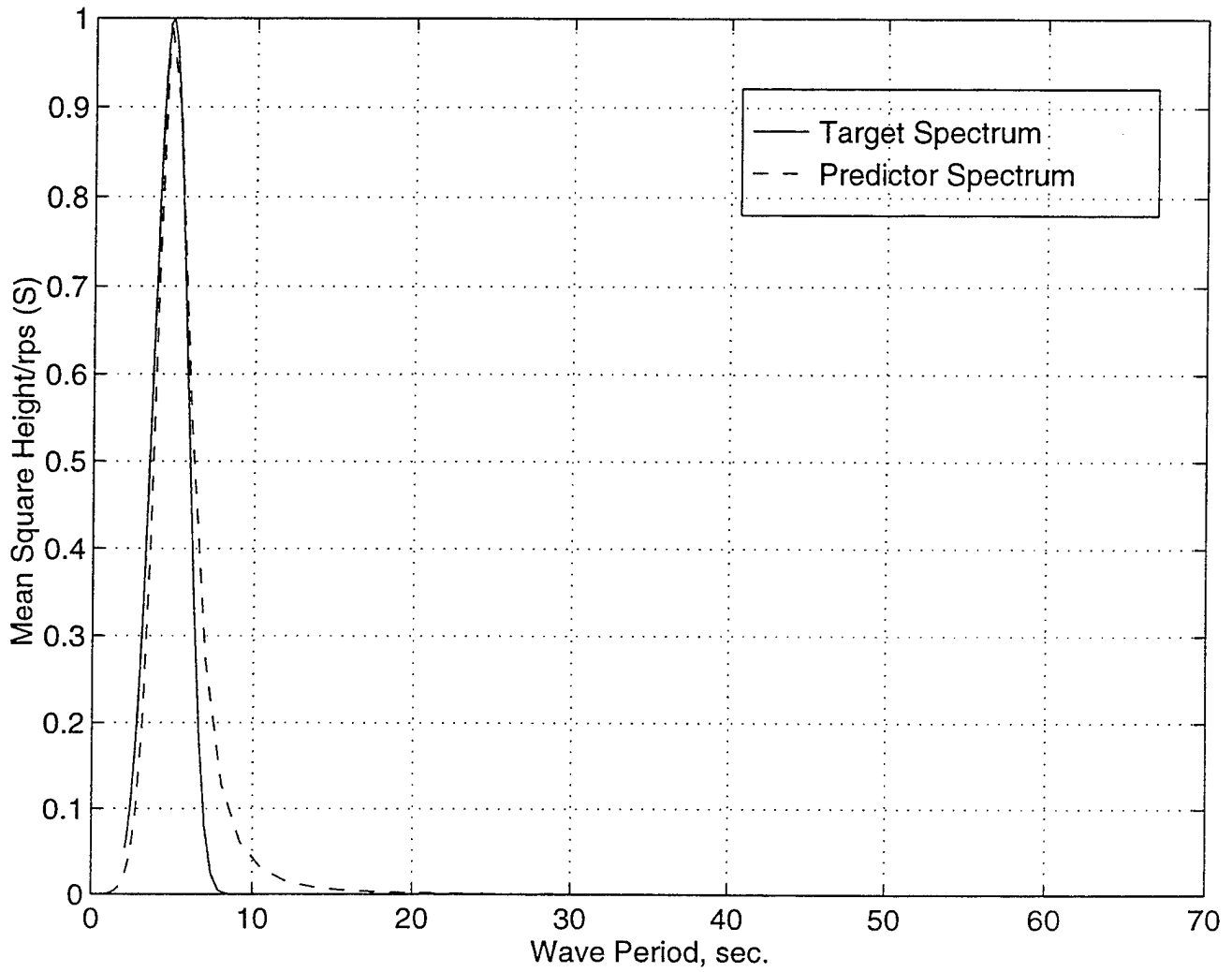


Figure 16. Predictor Spectrum versus P-M Spectrum.

The filter innovator (gain matrix  $K$ ) for this system was generated by using the LQR for determining the stability of the system. The frequency was chosen according to the peak frequency of the target wave spectrum. This value was determined to be approximately 1.31 rad/sec. It is worthwhile to note that the peak frequency for the P-M and P-M/pressure profile spectra was approximately 1.2 rad/sec. This frequency value, even though the difference is relatively small when comparing to that of the P-M spectrum alone, didn't match the target spectrum as well as the frequency of the P-M spectrum.

Tests conducted with the dynamic system using the two different peak frequencies were conducted. The frequency from the P-M spectrum predicted sea condition out to a further time with better accuracy. The filter gains for the LQR system were generated to match the target wave spectrum. Noticeable was the small difference between the filter of the pressure and target spectrum.

For this work, significant wave height of 3 feet was used for both the P-M target spectrum and pressure profiles. Figures 17 through 20 illustrate the frequency and period plots, depicting the significant wave height at this particular depth, for each spectrum. Figures 21 and 22 illustrate the relationship between the P-M spectrum pressure profiles by normalizing and superimposing them on the same plot. Figures 23 through 25 represent time records of the P-M spectrum, pressure profiles, and eight-order filter spectrum respectively. When comparing figure 25 to figure 9 (Spanos dimensionless time record), it is obvious that they differ immensely. The  $a_i$  and  $b_i$  coefficients of the eighth-order filter are listed in Table 3.

Number	Coefficient ( $b_i$ )	Coefficient ( $a_i$ )
0	0.1388	-
1	0.5684	-
2	1.7826	-
3	3.39	-
4	5.2488	0.3725
5	5.5542	0
6	4.7852	0
7	2.5	0
8	1	0

Table 3. Eighth-Order Filter Coefficients.

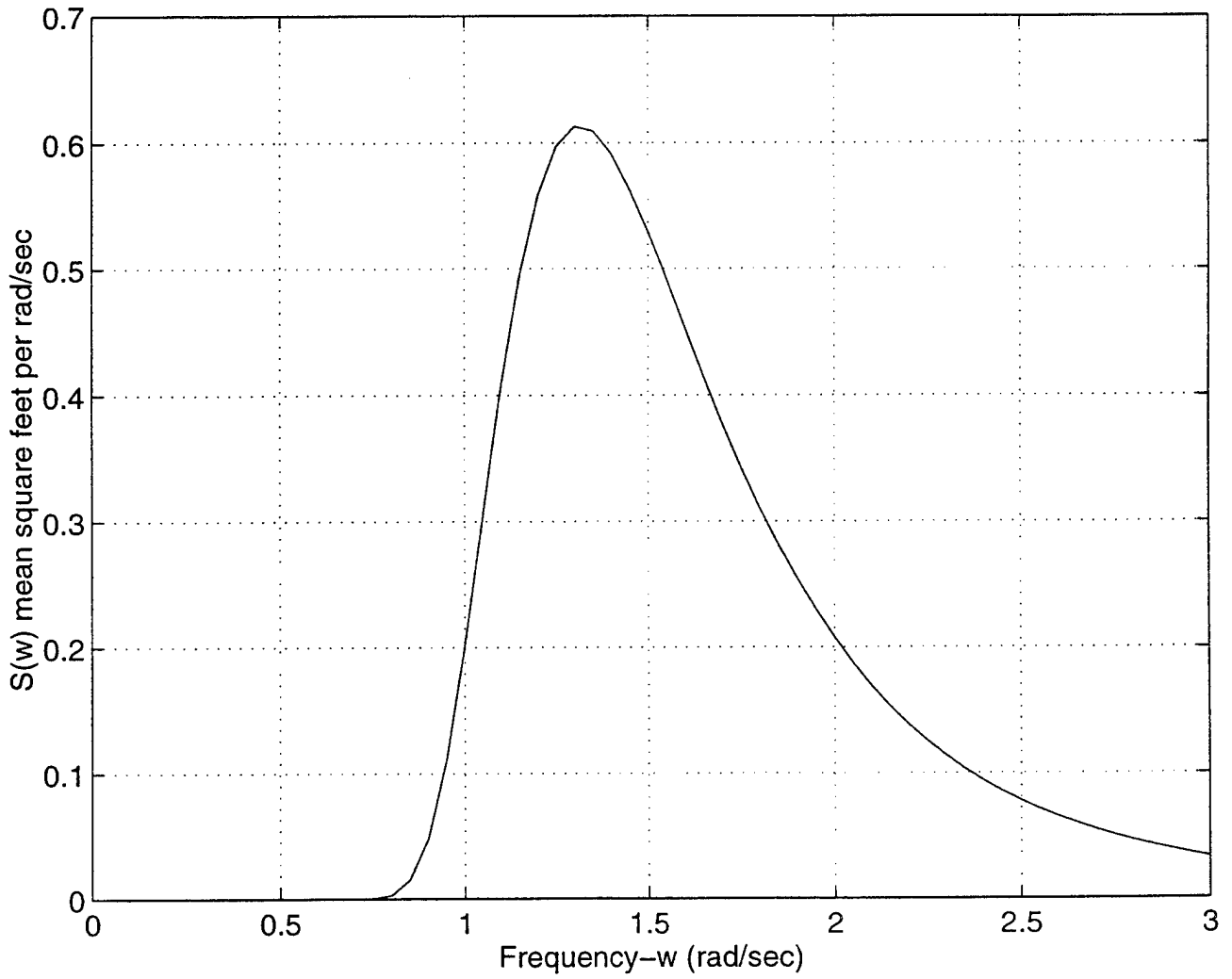


Figure 17. Frequency plot of P-M Wave Spectrum for significant wave height ( $H_{1/3}$ ) of 3 feet.

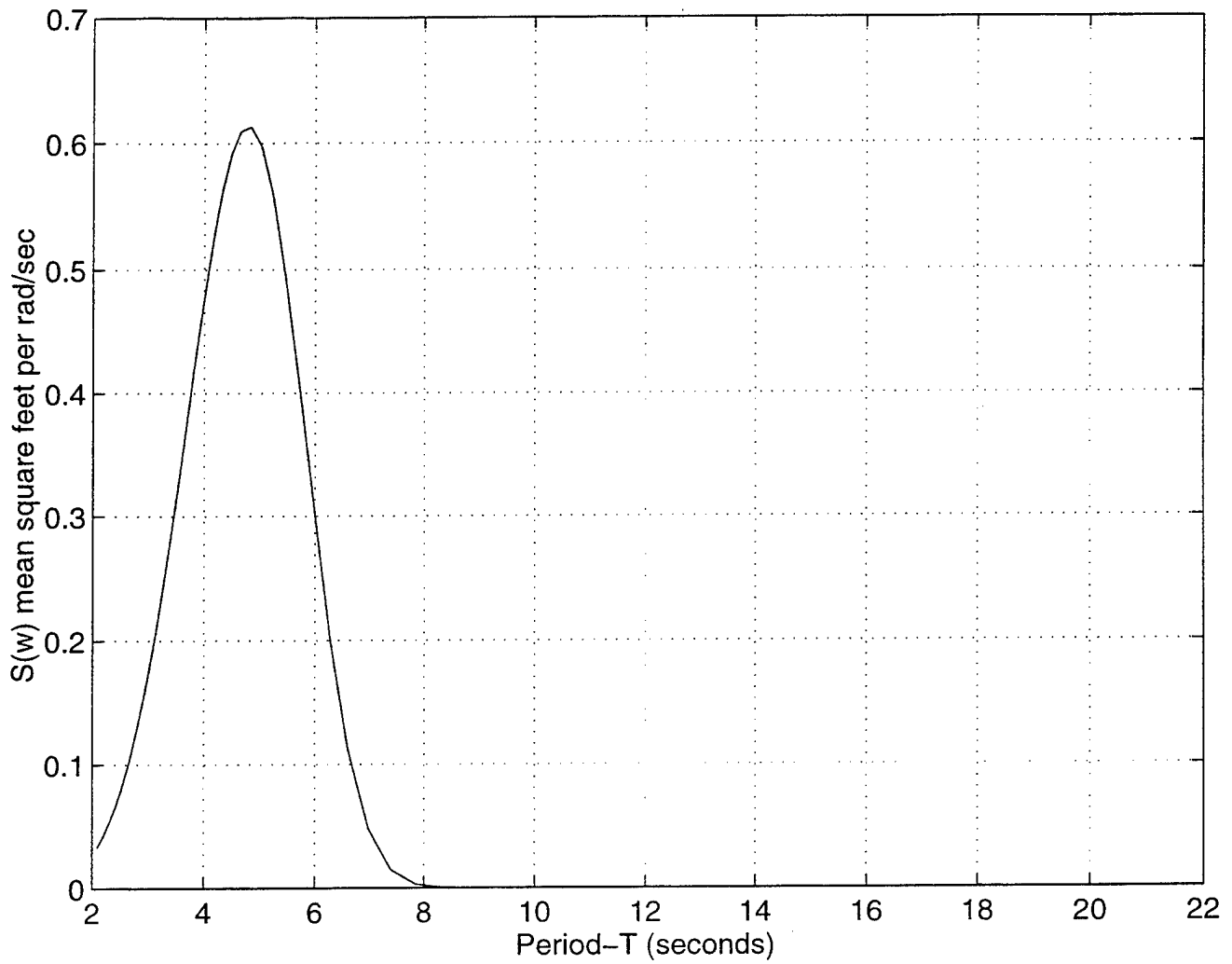


Figure 18. Period plot of P-M Wave Spectrum for significant wave height ( $H_{1/3}$ ) of 3 feet.

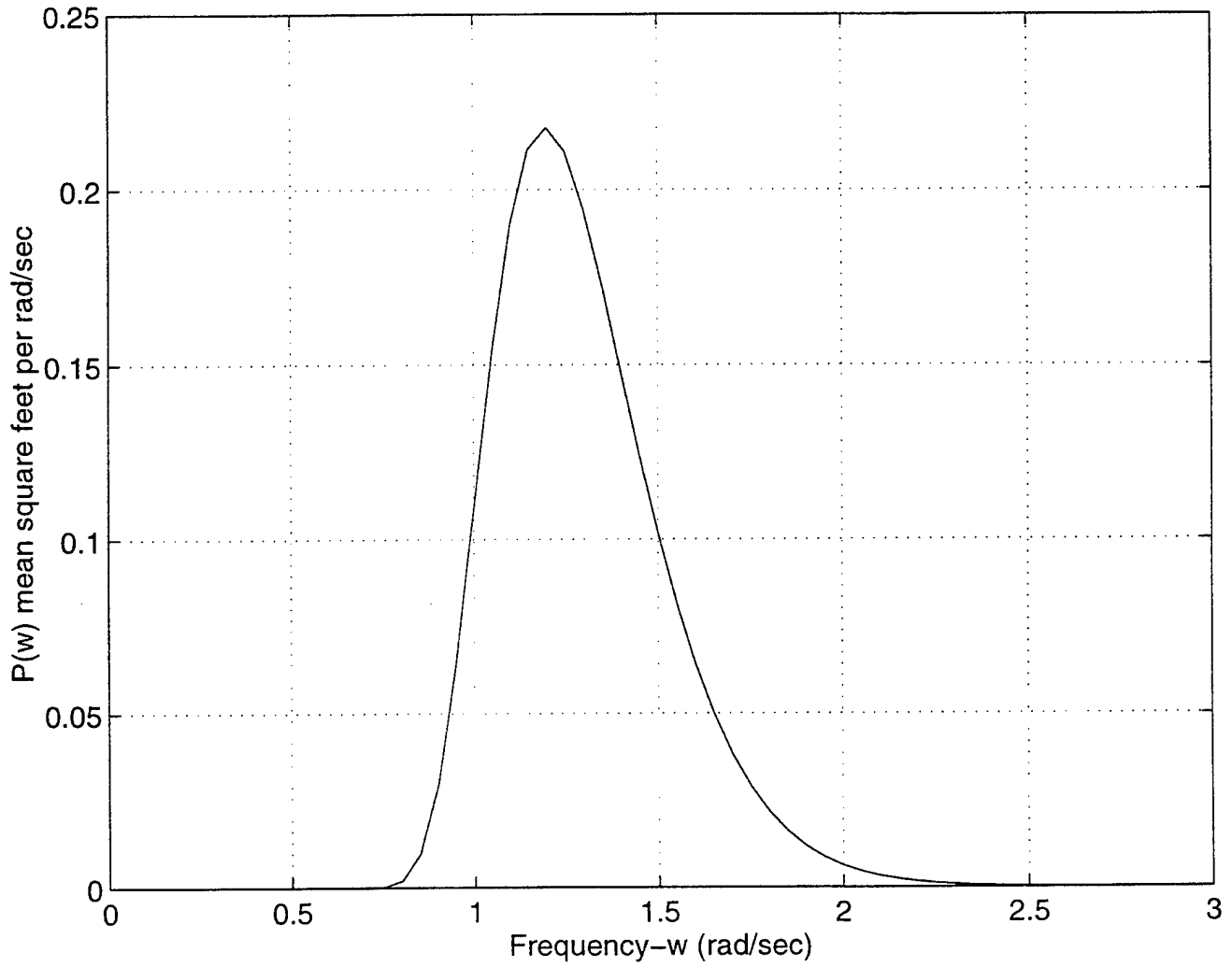


Figure 19. Frequency plot of Pressure Profile Spectrum for significant wave height ( $H_{1/3}$ ) of 3 feet.

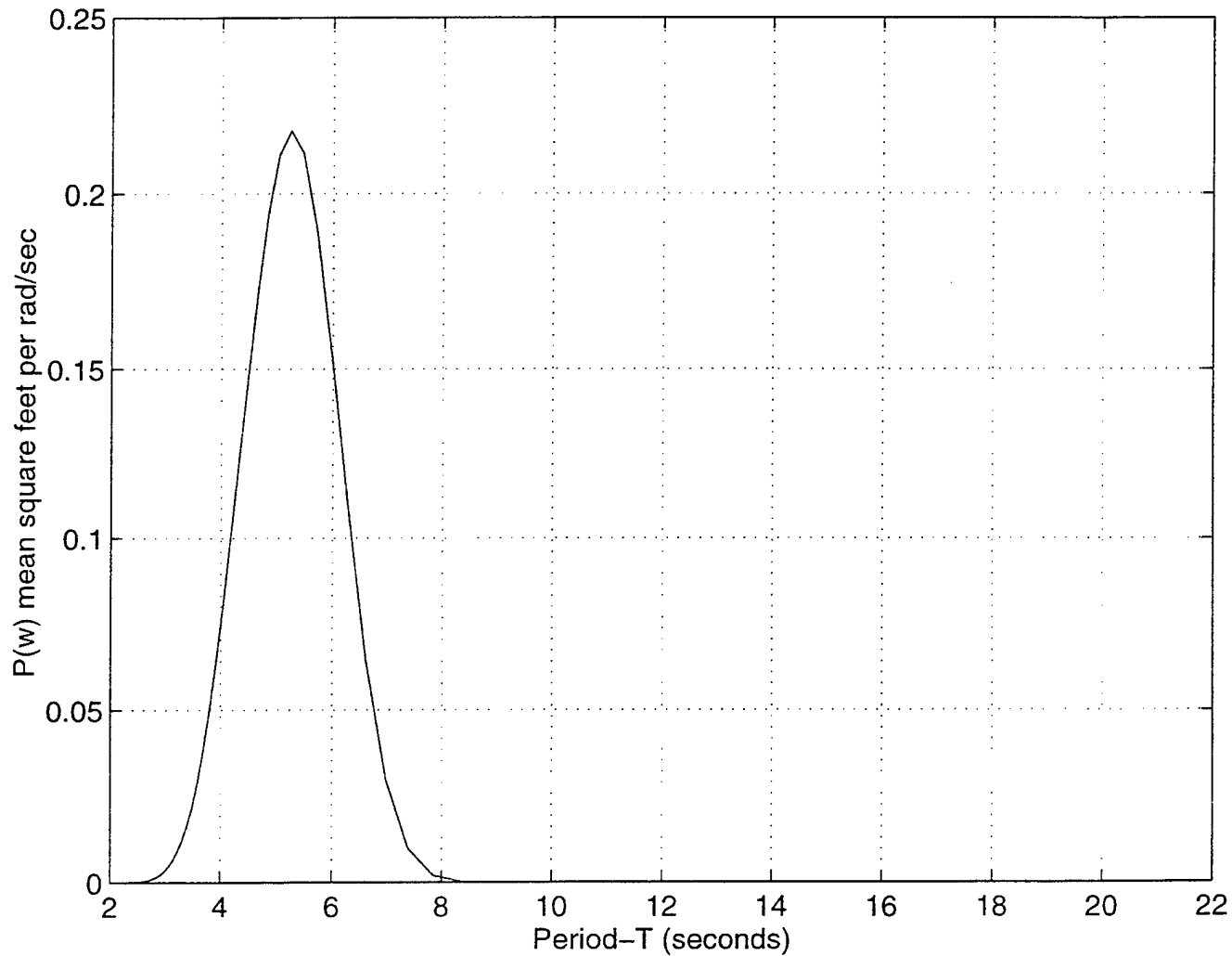


Figure 20. Period plot of Pressure Profile Spectrum for significant wave height ( $H_{1/3}$ ) of 3 feet.

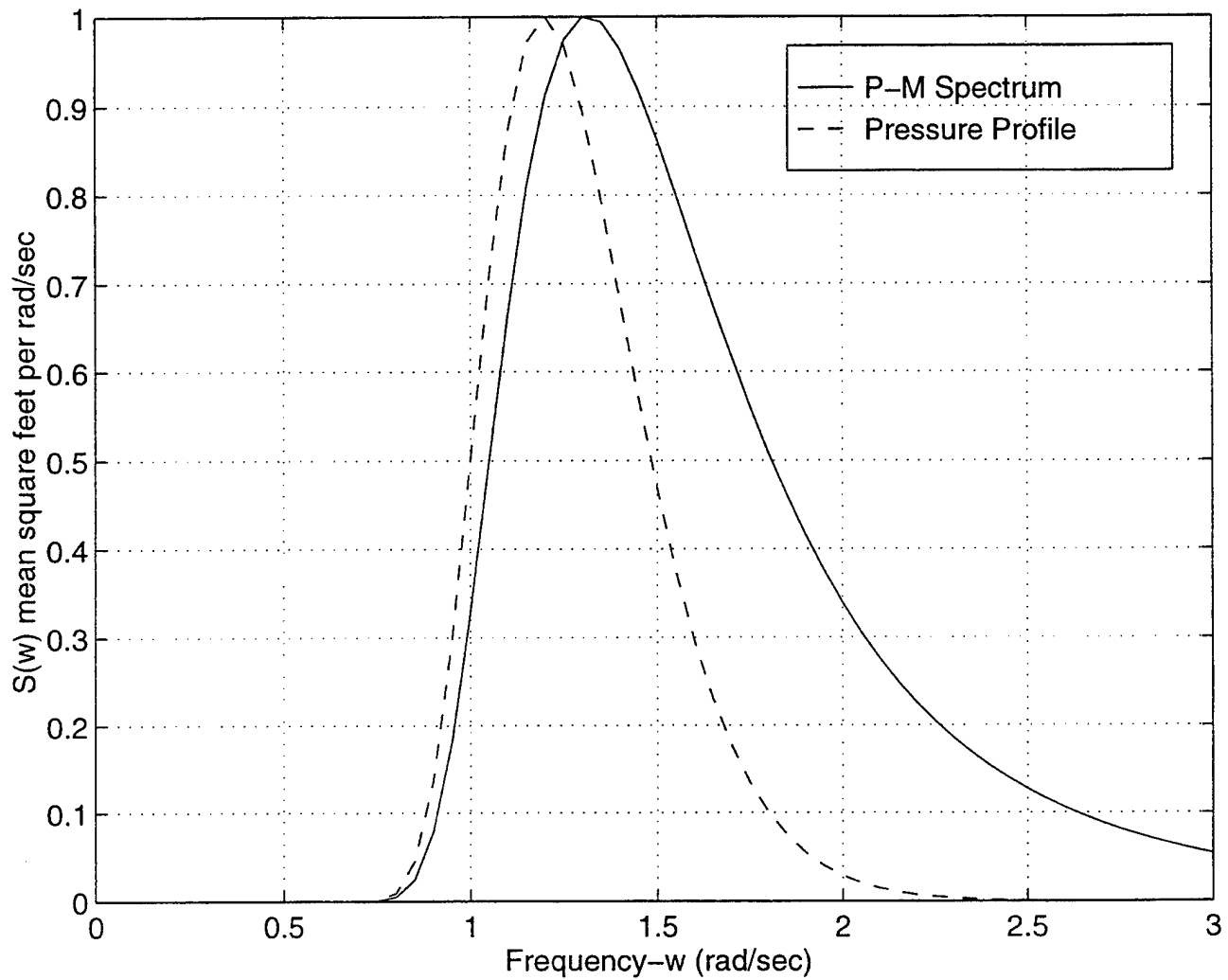


Figure 21. Frequency plot P-M spectrum superimposed on Pressure Profile Spectrum for significant wave height ( $H_{1/3}$ ) of 3 feet (normalized spectra).

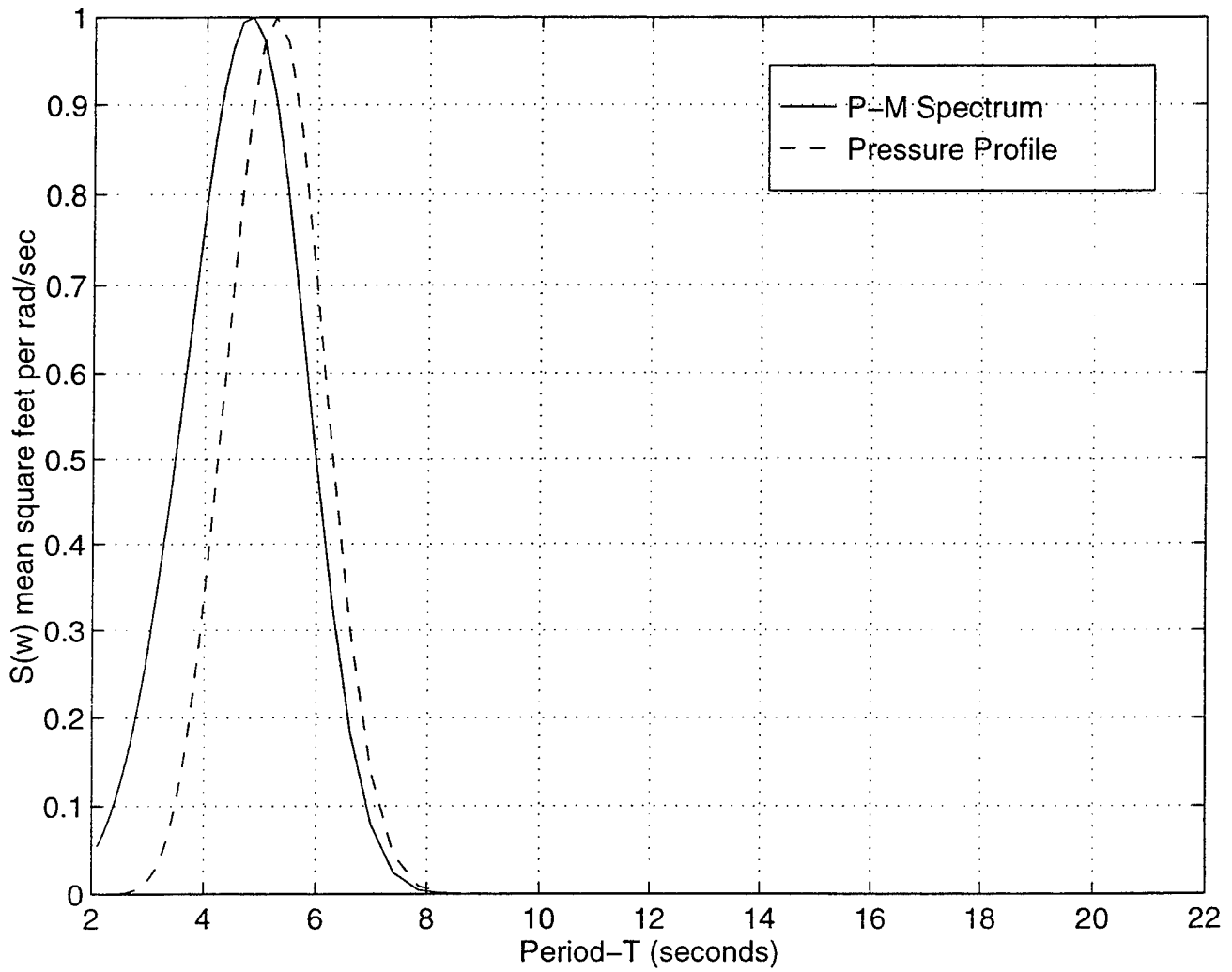


Figure 22. Period plot P-M spectrum superimposed on Pressure Profile Spectrum for significant wave height ( $H_{1/3}$ ) of 3 feet (normalized spectra).

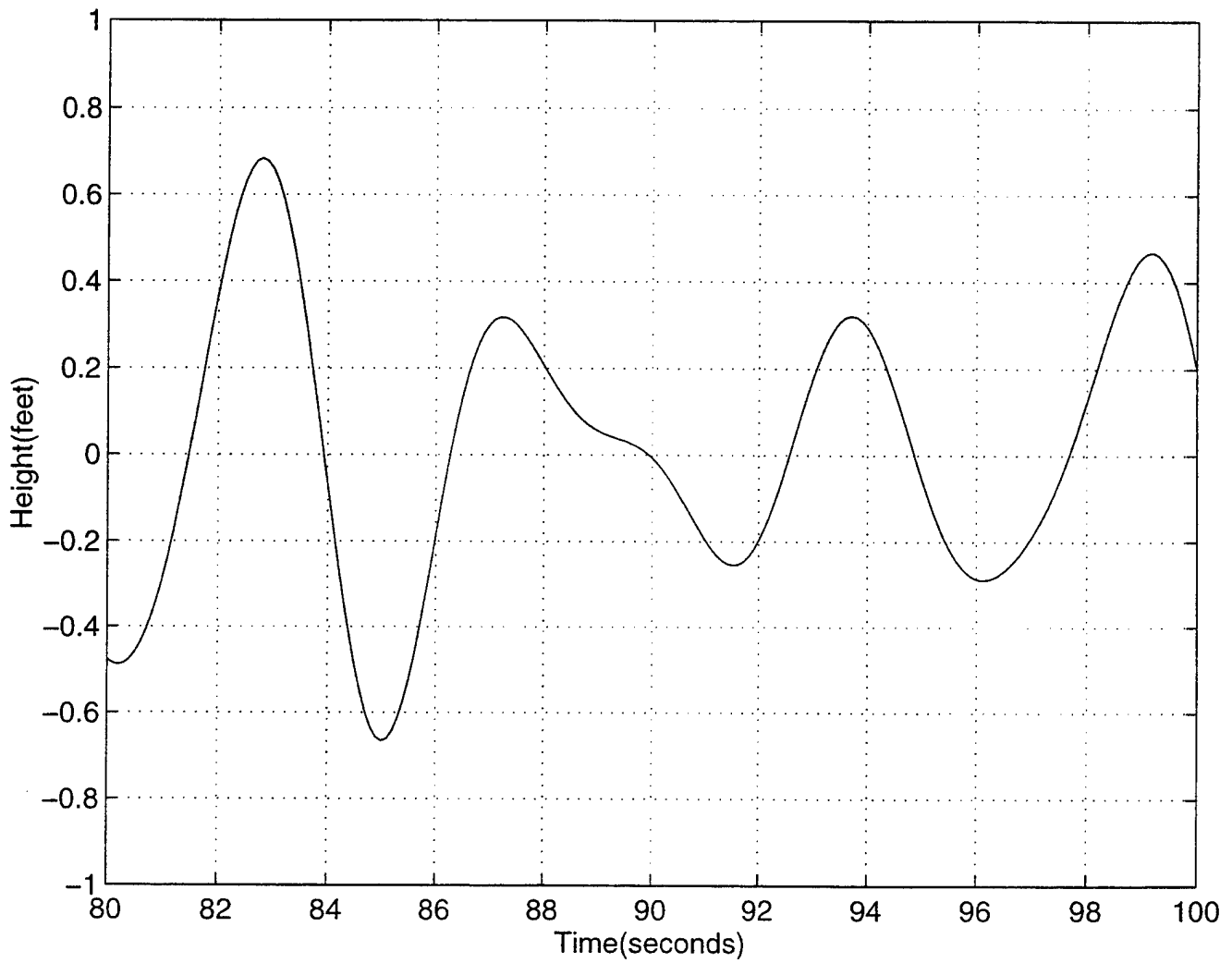


Figure 23. Time History of Pierson-Moskowitz Spectrum reflecting random output for significant wave height ( $H_{1/3}$ ) of 3 feet.

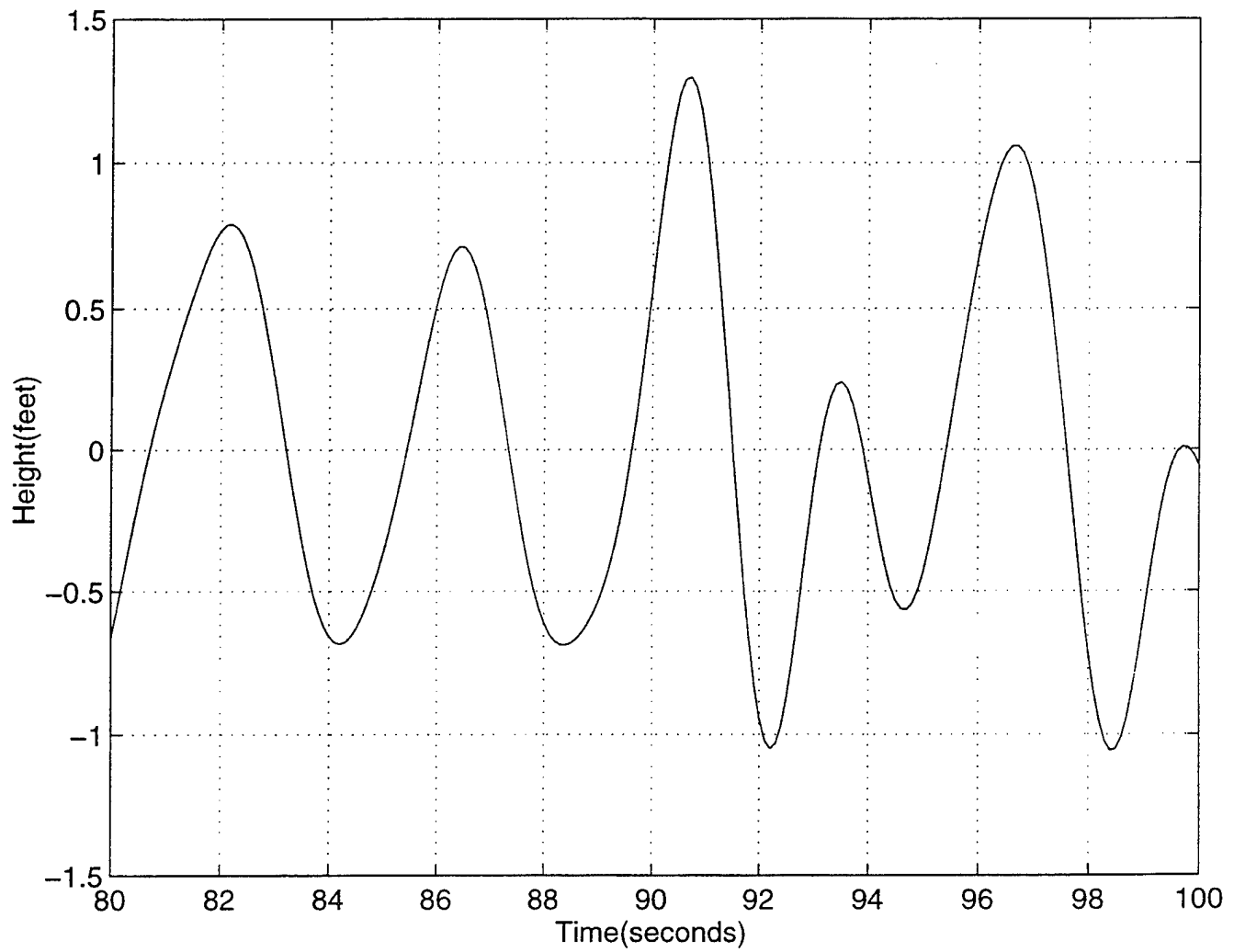


Figure 24. Time History of Pressure Profiles reflecting random output for significant wave height ( $H_{1/3}$ ) of 3 feet.

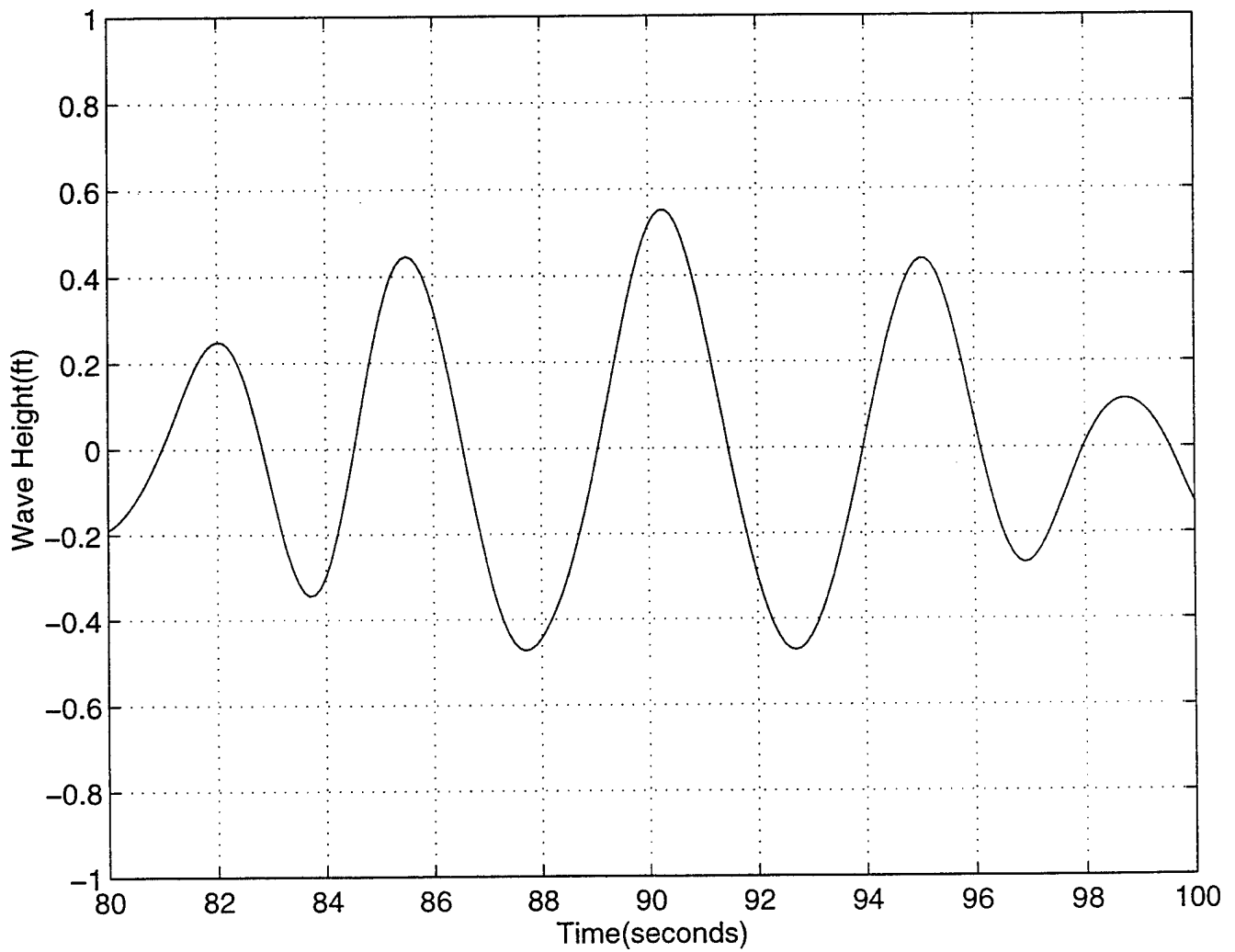


Figure 25. Time History of Measured Pressue Profile reflecting random output of eighth-order, digital filter for significant wave height ( $H_{1/3}$ ) of 3 feet.



#### IV. RESULTS

To aid in the discussion of results, it is helpful to give the following,

Definition:

$\hat{p}(t, (t + \tau))$ : estimate of forward pressure at time,  $(t + \tau)$  predicted at current time,  $(t)$ .

$y(t)$ : measured pressure at time,  $(t)$ .

$y(t + \tau)$ : measured pressure to be found from seastate at time,  $(t + \tau)$ .

Prediction error,  $(\epsilon_o)$  at time,  $(t + \tau)$  based on filter data up to time  $(t)$ :

$$\epsilon(t, (t + \tau)) = \hat{p}(t, (t + \tau)) - y(t + \tau)$$

Figure 26 illustrates how this error is defined graphically while Figures 27 through 38 graphically reflect time history plots of the results obtained from the above definitions.

A measure of effectiveness is the forward prediction using the correlation coefficient between digital output of the P-M/pressure profile target spectrum and transfer function of eighth-order system. This measure of effectiveness predicted wave and pressure responses out to designated number of time steps (number of time steps for each measure is reflected on plots of the results). However, in this work, results were taken at time,  $\tau=5$  and  $\tau=30$  seconds. A fluctuation was observed with the cross-correlation results. This fluctuation is mostly believed to be the aftermath of the random phenomenon of the seaway time history record which had to be modeled with a random white noise output process of a digital filter. As a measure to compensate for the fluctuation and

obtain the best results, the output data were calculated fifty iterations and averaged to get the final data value. The graph in figure 39 depicts the mean cross-correlation coefficient flanked by the standard deviation.

$p(t + \tau)$  and  $\hat{p}(t + \tau)$  were compared over the entire time record, while the following expression was used to formulate the cross-correlation coefficient.

$$\rho(\tau) = \frac{\sum_{t=1}^N p(t + \tau)\hat{p}(t, t + \tau) / N}{std(p)std(\hat{p})}$$

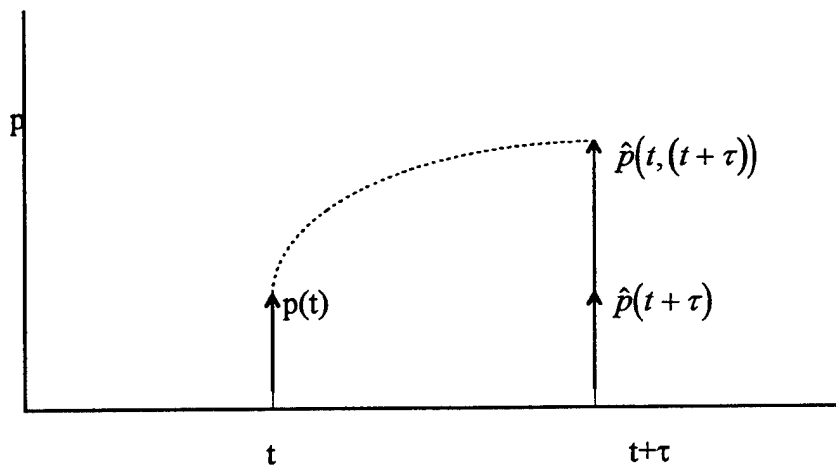


Figure 26. Forward Prediction Diagram

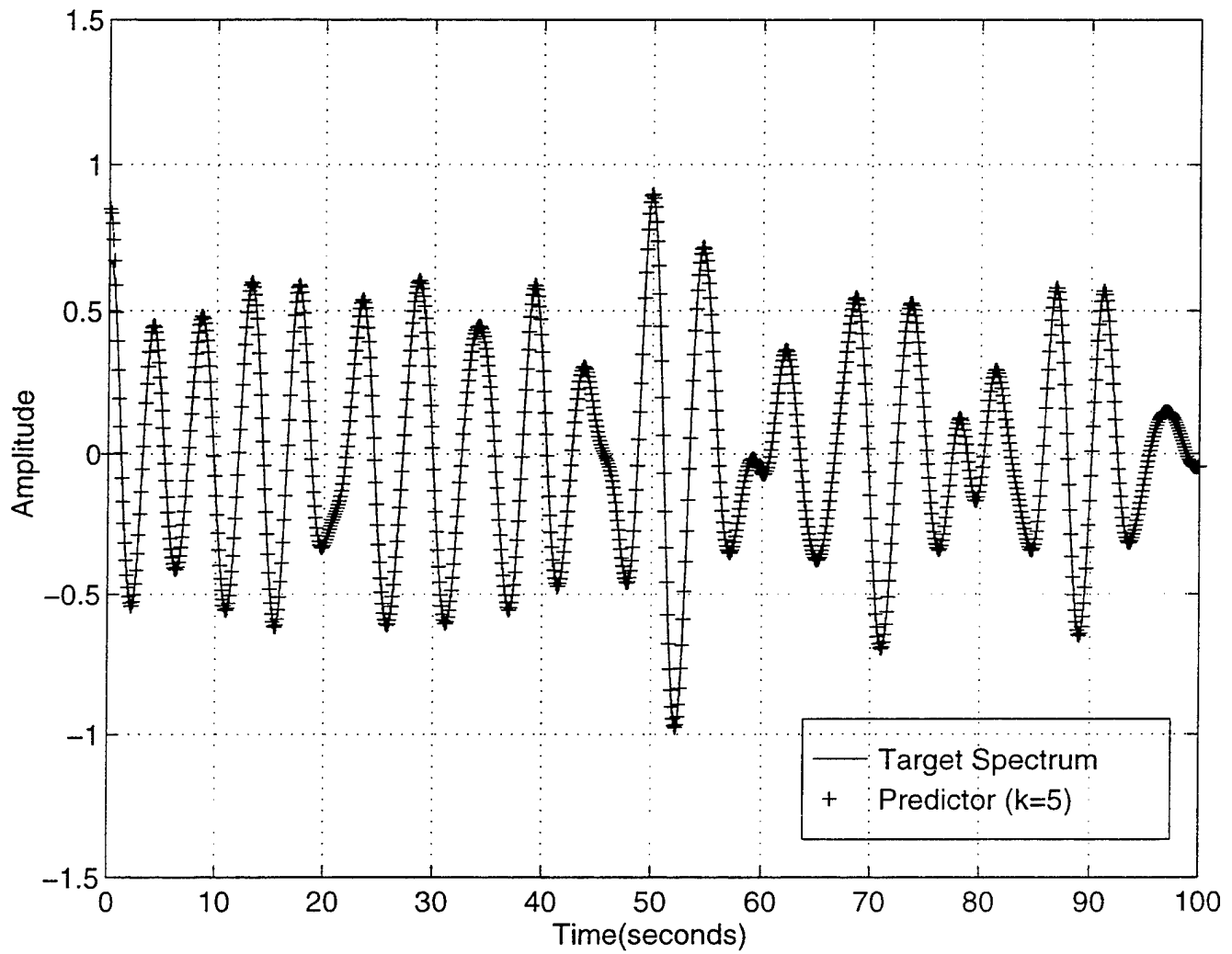


Figure 27. Time Record of P-M Target Spectrum ( $Y$ ) versus Measured Pressure ( $p$ ), (Predictor).

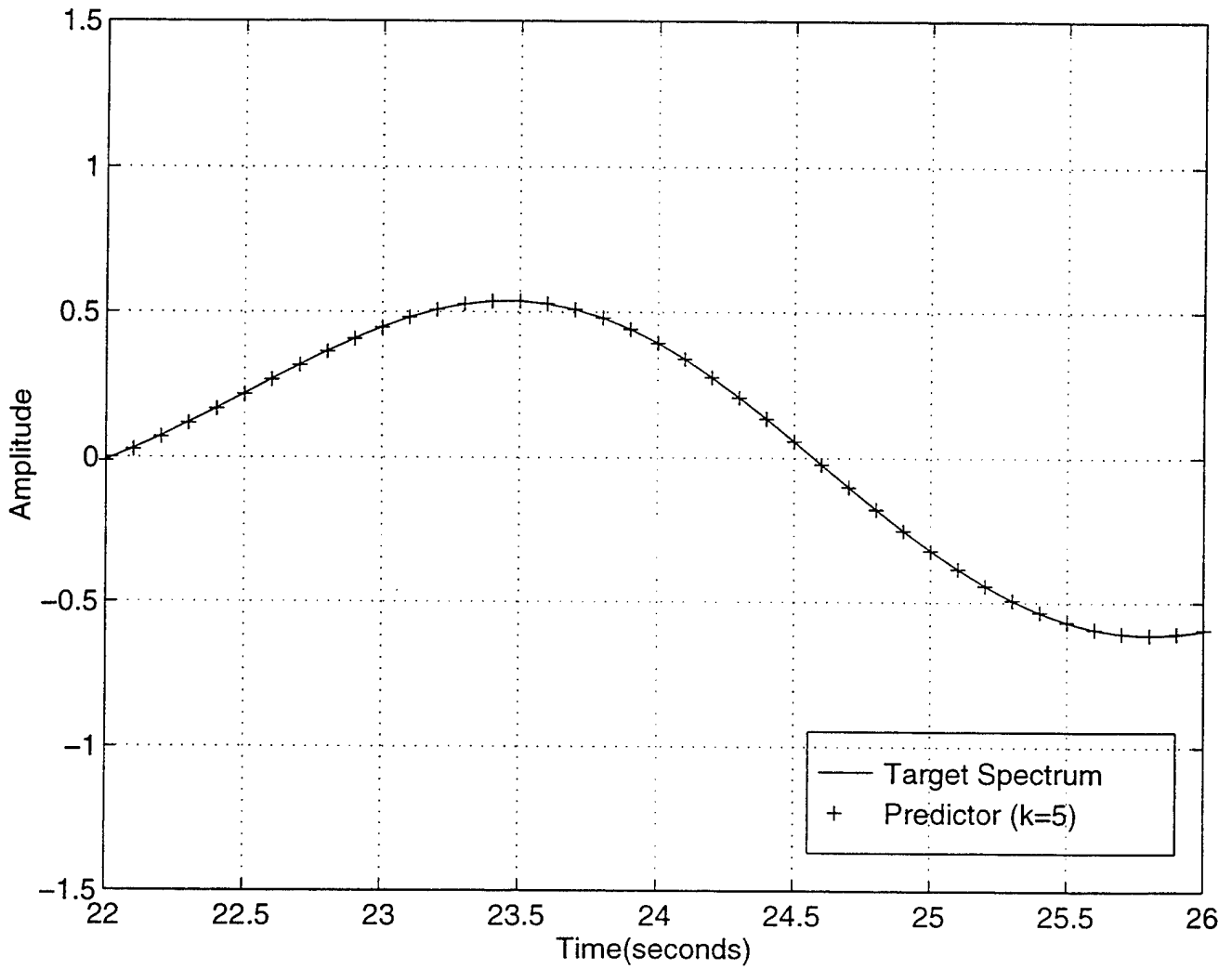


Figure 28. Zoomed Plot of Time Record of P-M Target Spectrum ( $Y$ ) versus Measured Pressure ( $p$ ), (Predictor).

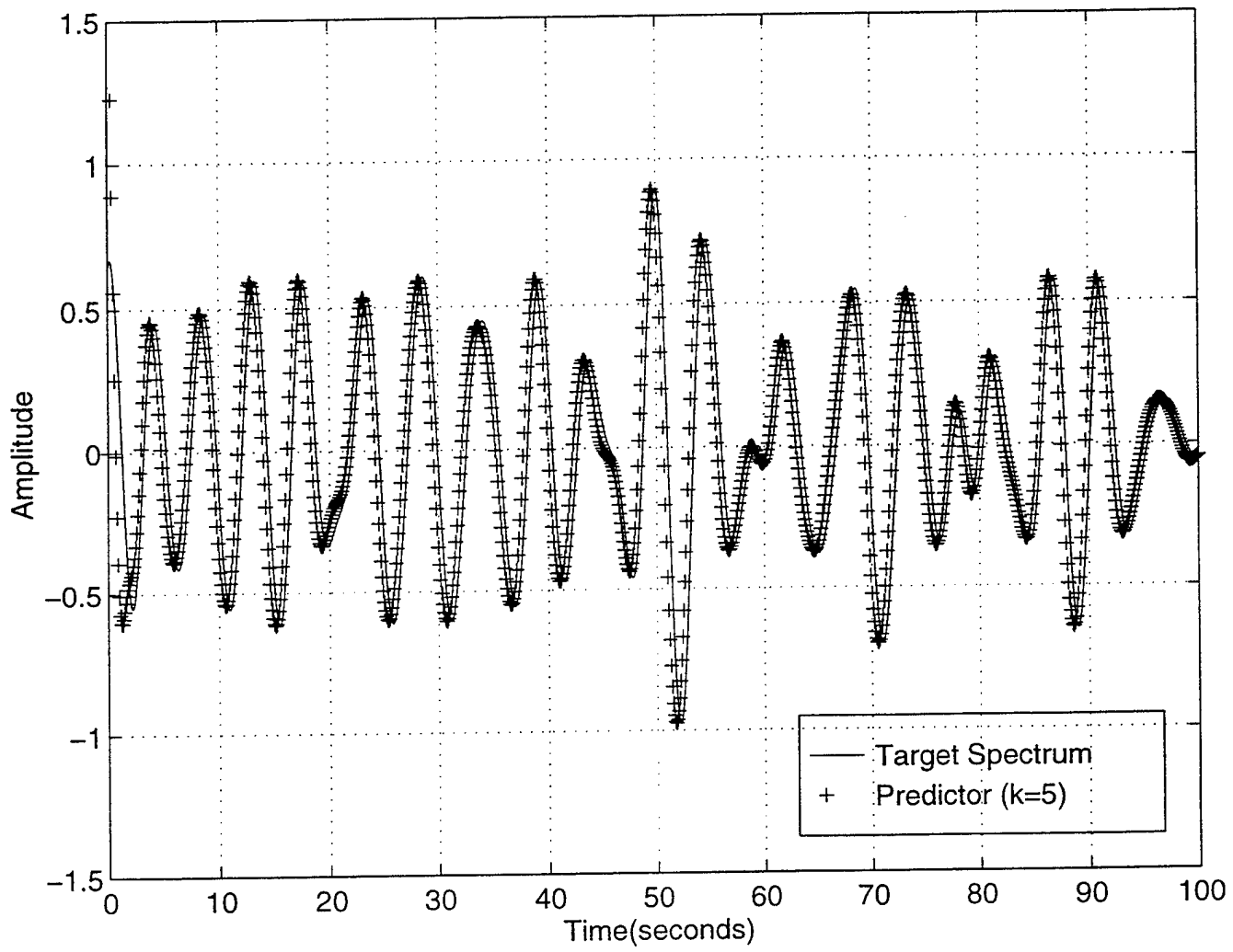


Figure 29. Time Record of Measured Pressure ( $p$ ) versus Measured Pressure  $p(t+\tau)$ .

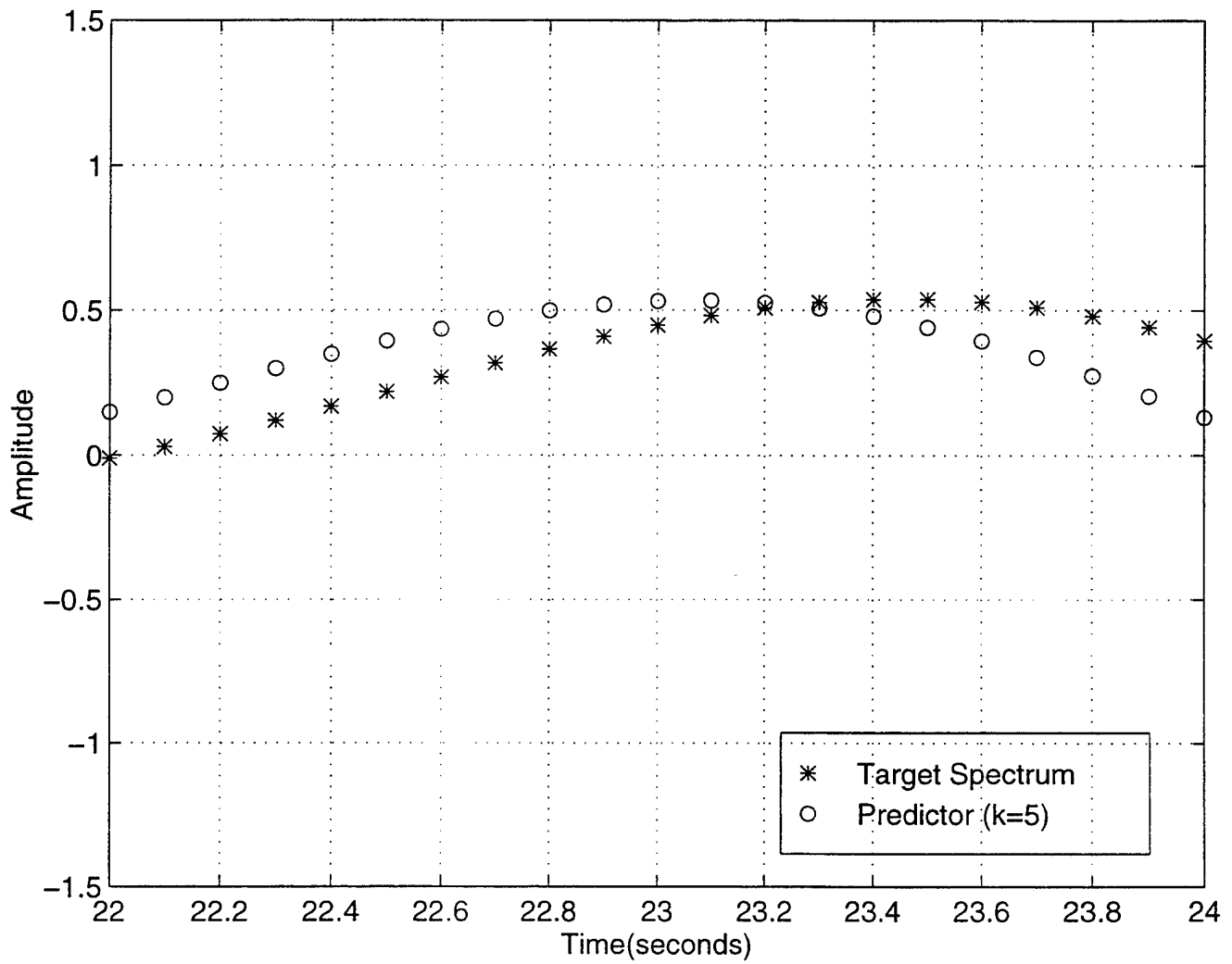


Figure 30. Zoomed Plot of Time Record of Measured Pressure ( $p$ ) versus Measured Pressure  $p(t+\tau)$ .

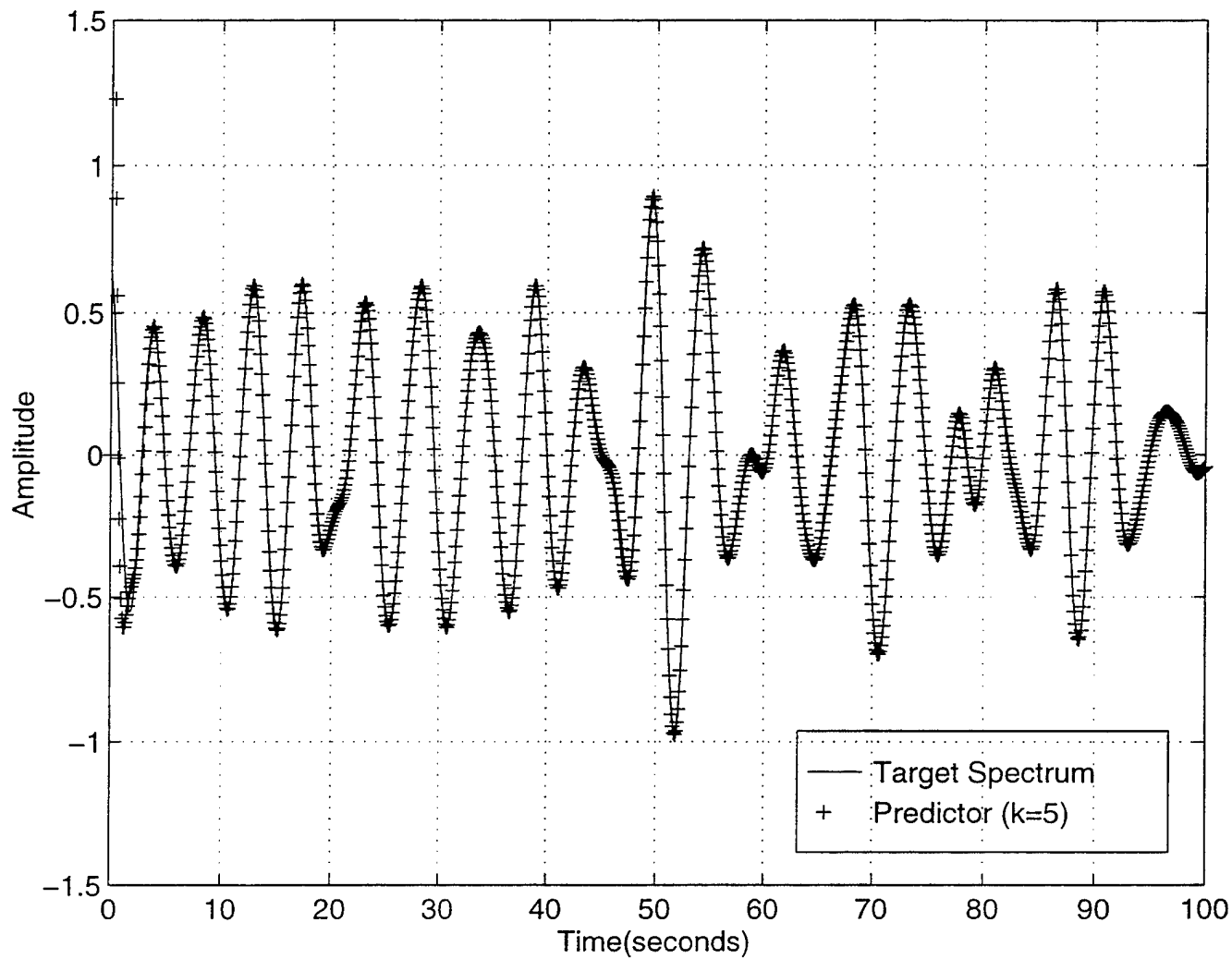


Figure 31. Time Record of Measured Pressure  $p(t+\tau)$  versus Estimate of Forward Pressure  $\hat{p}(t,(t+\tau))$ .

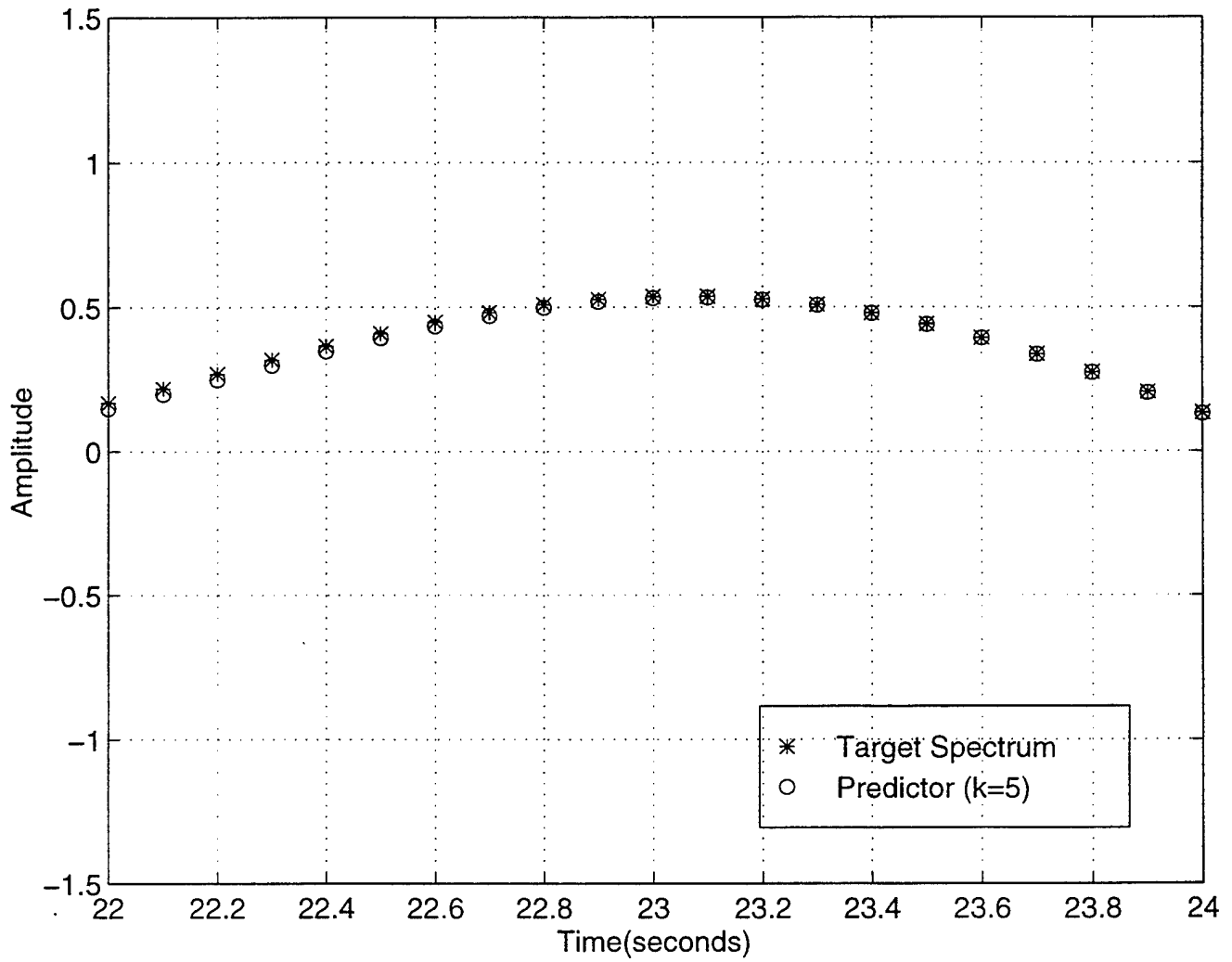


Figure 32. Zoomed Plot of Time Record of Measured Pressure  $p(t + \tau)$  versus Estimate of Forward Pressure  $\hat{p}(t, (t + \tau))$ .

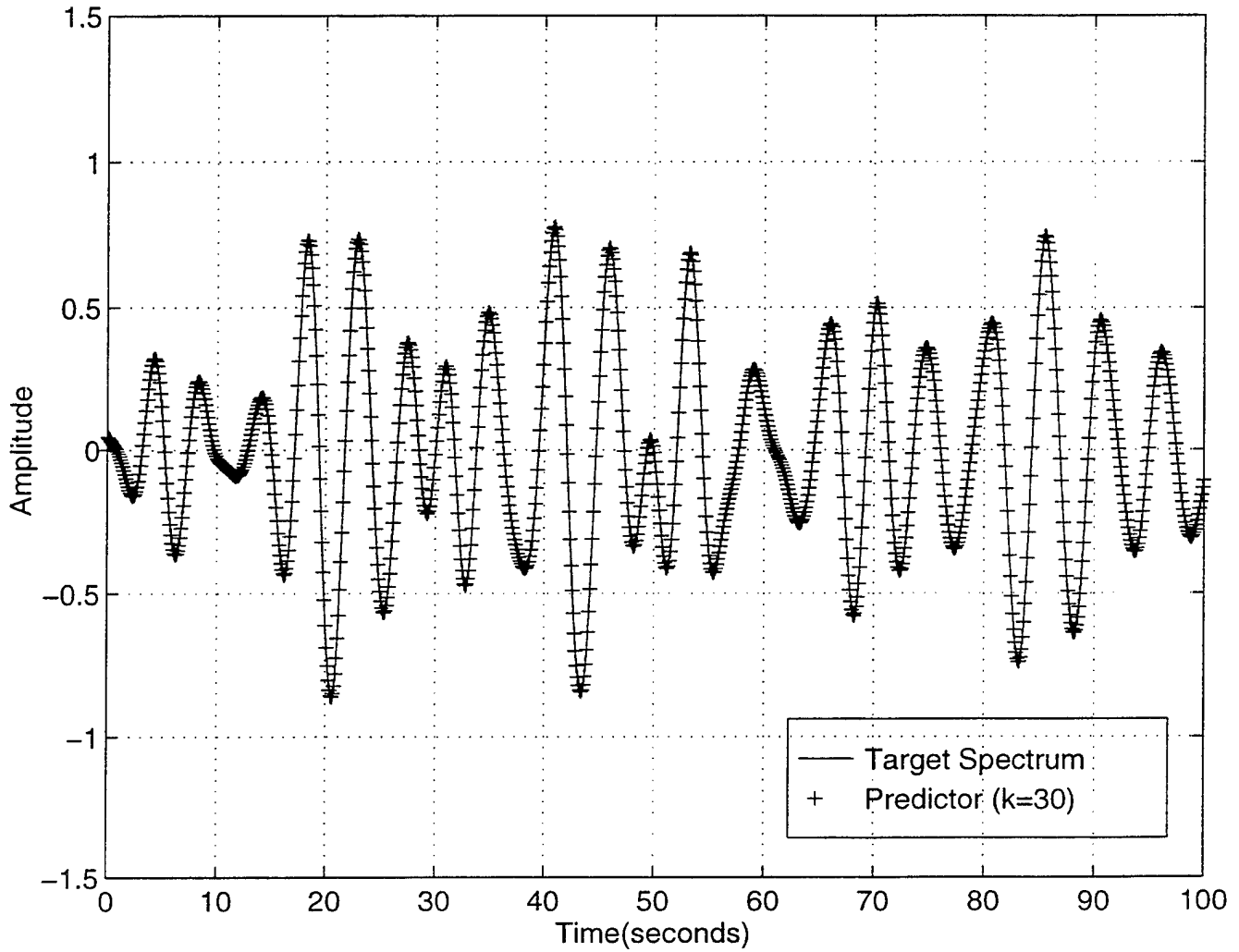


Figure 33. Time Record of P-M Target Spectrum ( $Y$ ) versus Measured Pressure ( $p$ ), (Predictor).

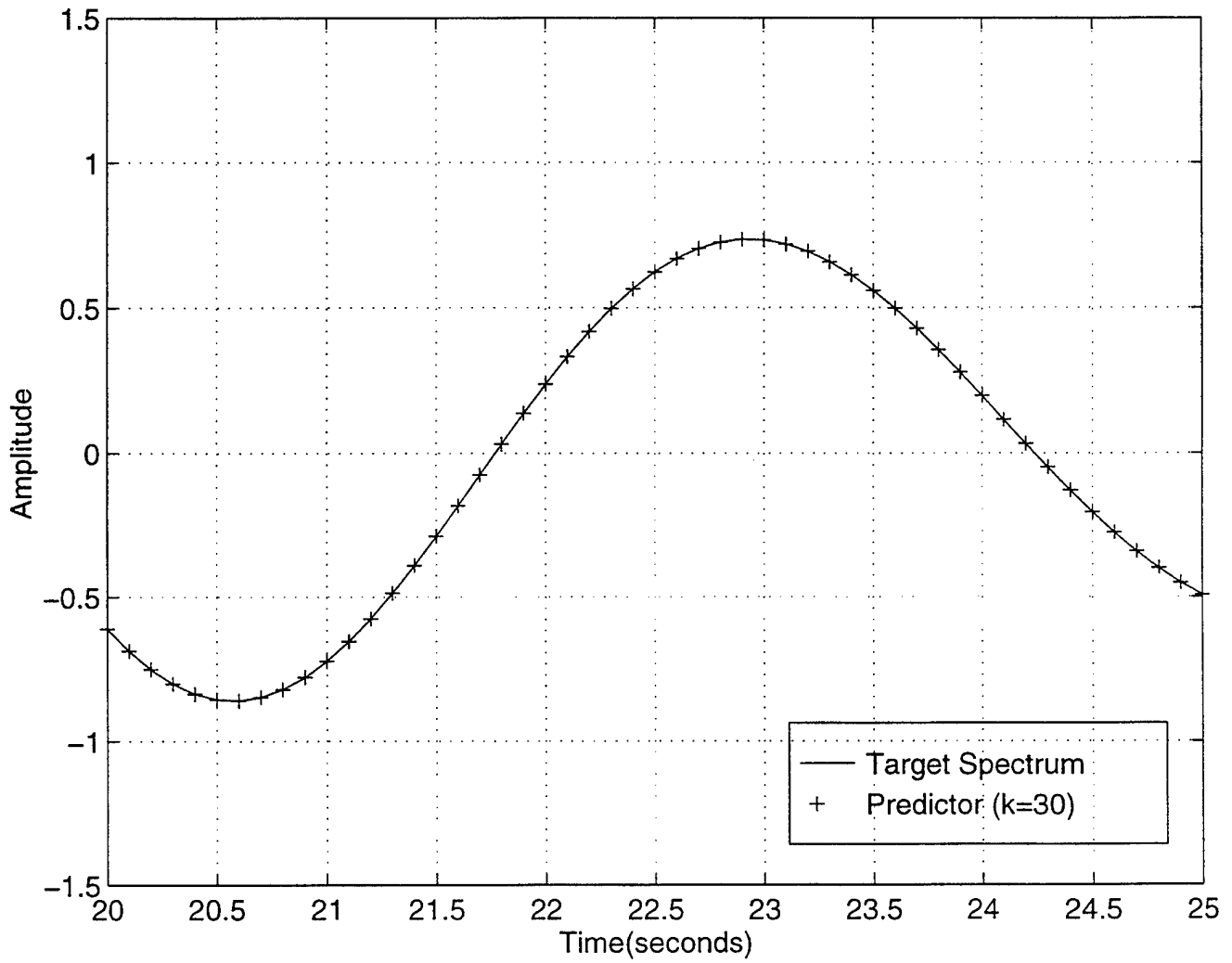


Figure 34. Zoomed Plot of Time Record of P-M Target Spectrum ( $Y$ ) versus Measured Pressure ( $p$ ), (Predictor).

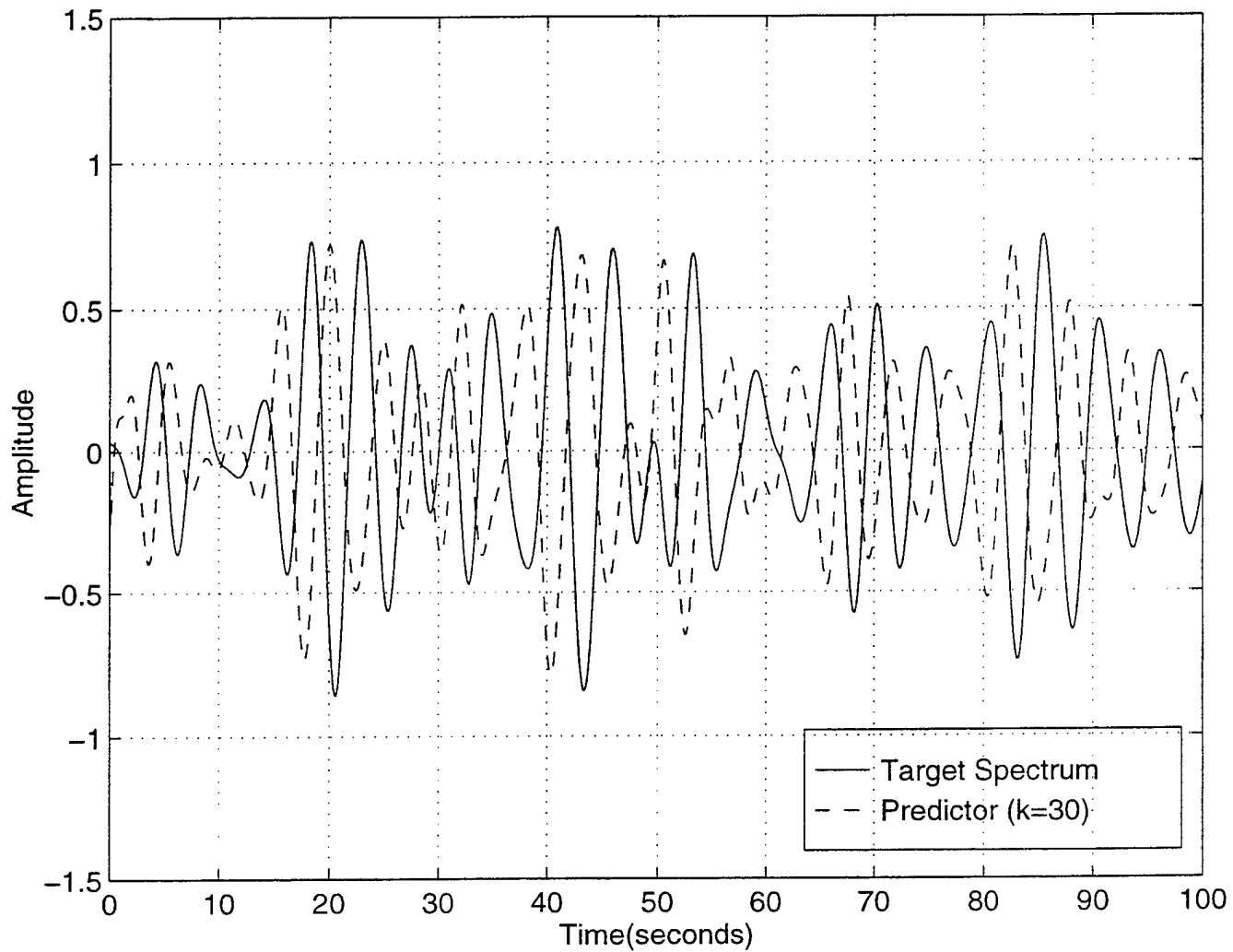


Figure 35. Time Record of Measured Pressure ( $p$ ) versus Measured Pressure  $p(t + \tau)$ .

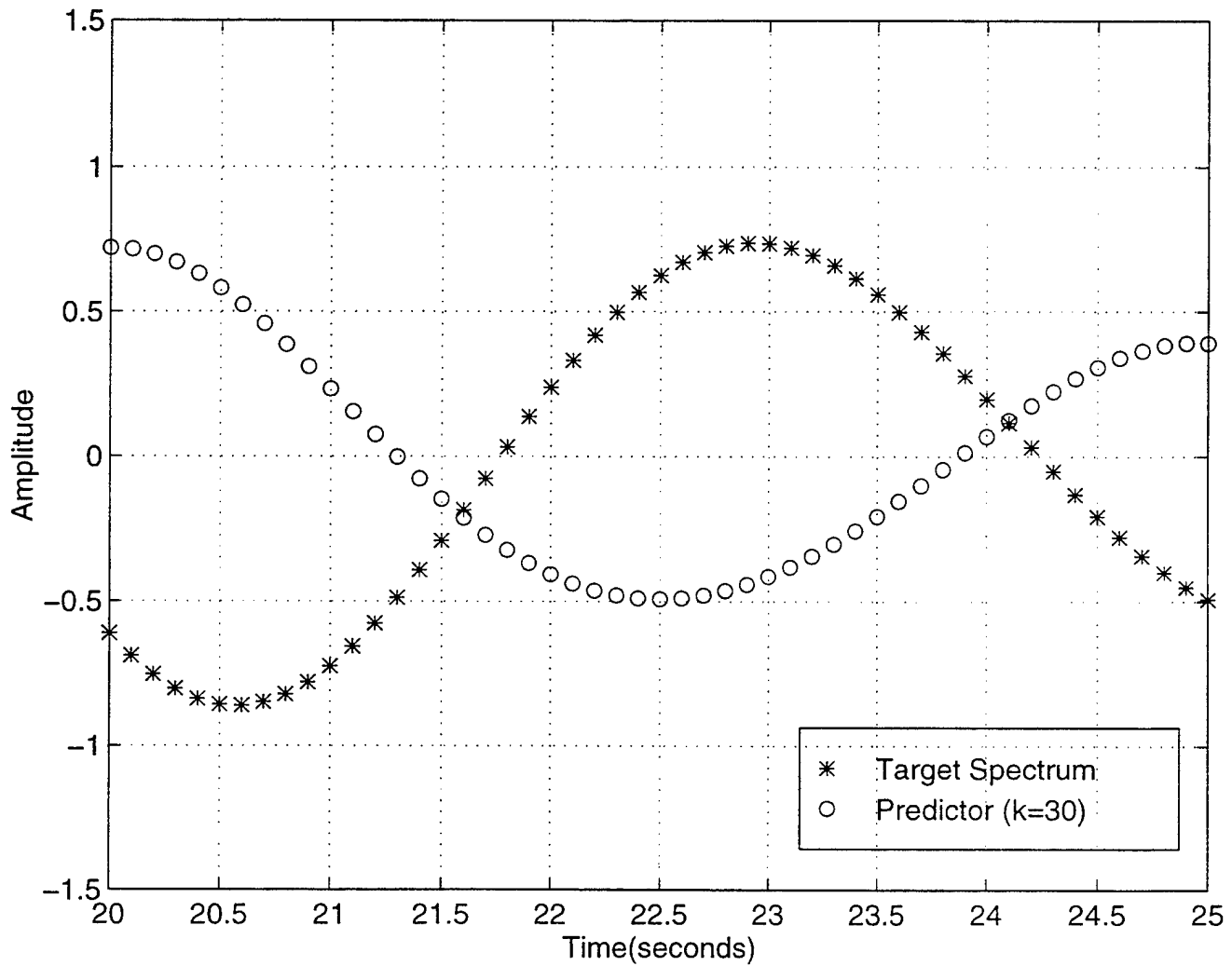


Figure 36. Zoomed Plot of Time Record of Measured Pressure ( $p$ ) versus Measured Pressure  $p(t + \tau)$ .

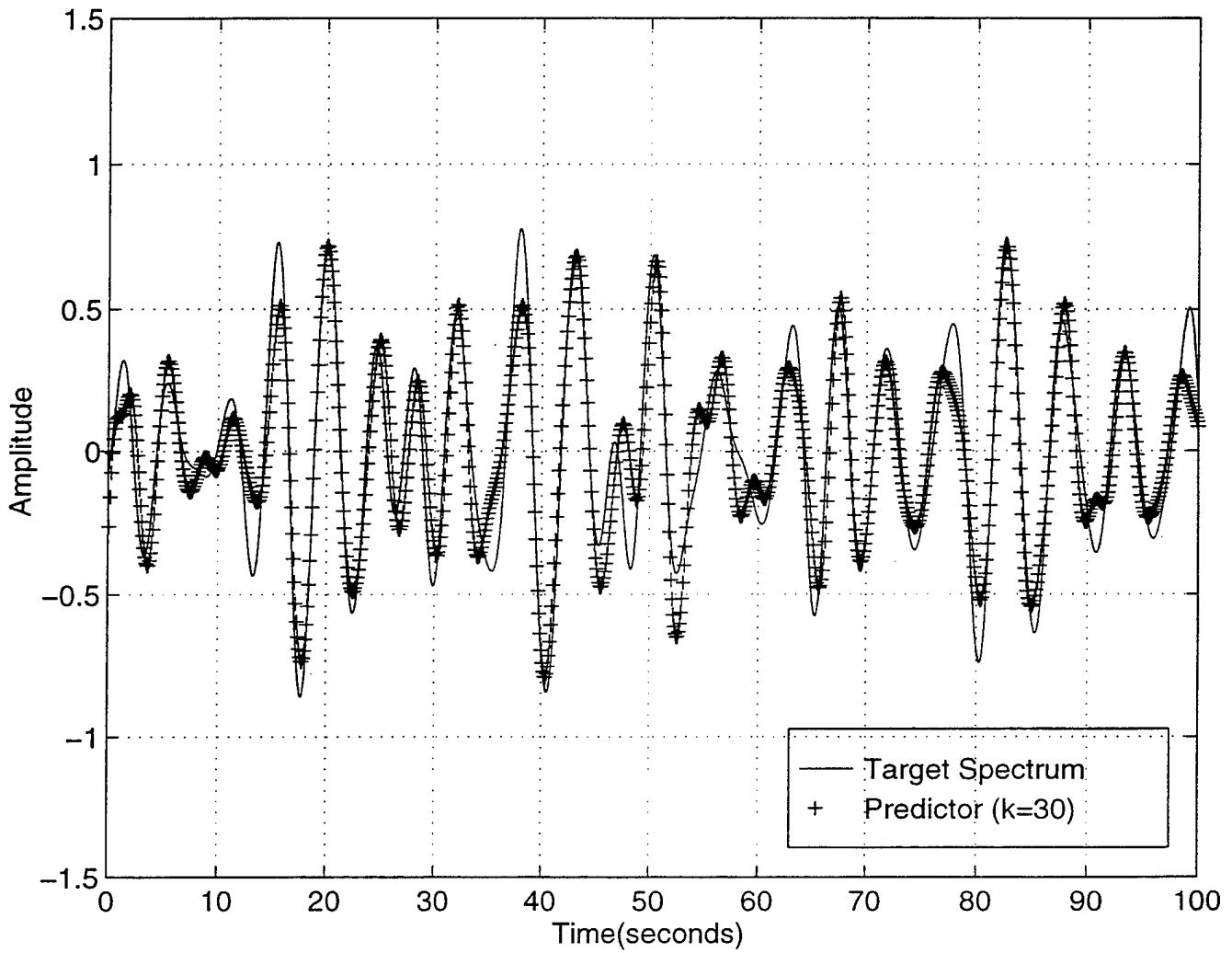


Figure 37. Time Record of Measured Pressure  $p(t+\tau)$  versus Estimate of Forward Pressure  $\hat{p}(t,(t+\tau))$ .

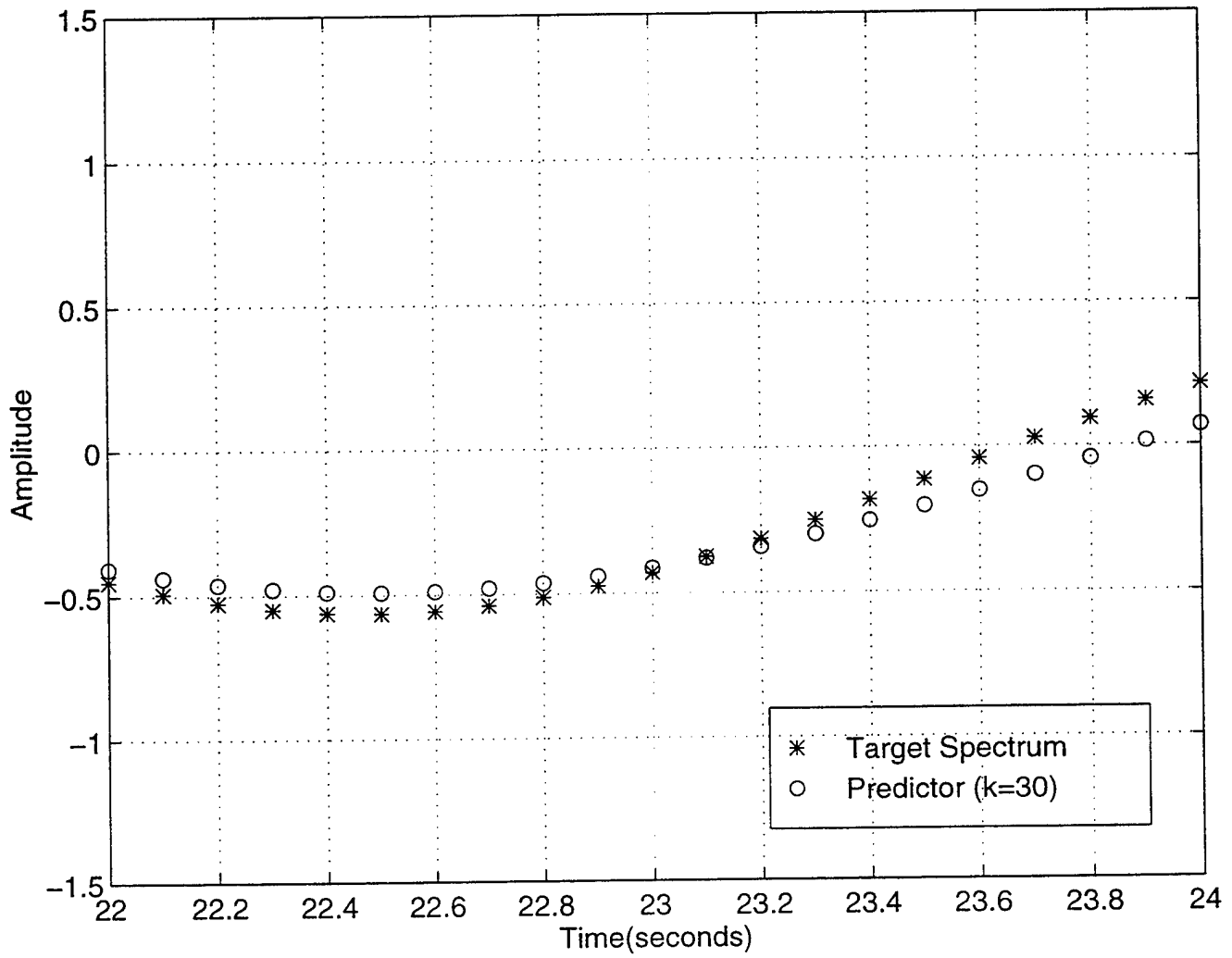


Figure 38. Zoomed Plot of Time Record of Measured Pressure  $p(t+\tau)$  versus Estimate of Forward Pressure  $\hat{p}(t, (t+\tau))$ .

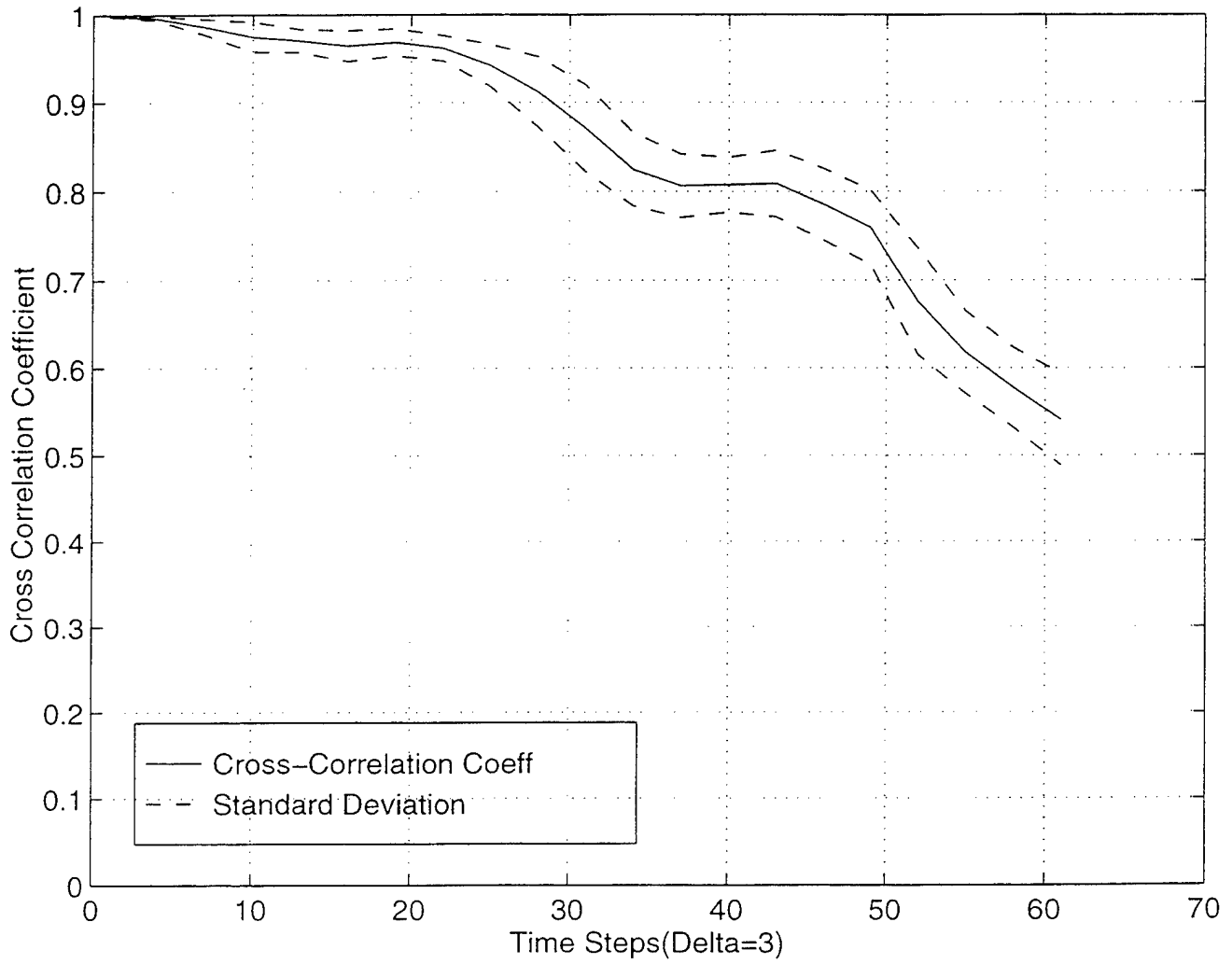


Figure 39. Mean Cross-Correlation Coefficient and Standard Deviation between P-M Target Spectrum and Digital Filter.

## V. CONCLUSION AND RECOMMENDATIONS

### A. CONCLUSION

In previous studies of hydrodynamic effects on underwater structures, attempts to simulate waves using the Pierson Moskowitz spectrum have long been of interest. This work has revealed that using an eighth-order filter is a convenient means of matching the P-M spectrum and predicting future seaway surface elevation behavior.

It was discovered that the application of normalized coefficients to model seaway for various states proved to be inconsistent with the actual behavior of sea waves. This discovery was explored when a comparison of spectral densities and time history plots between dimensionless and an eighth-order transfer function coefficients was made. From comparing the spectral densities and time history of Spanos' model and the eighth-order filter with the spectral density of the P-M spectrum, it became apparent that Spanos model failed to match the P-M spectrum while the eighth-order system proved to be promising, matching the P-M spectrum very closely.

It has been concluded that an eighth-order transfer function provides good coefficients for tracking the P-M target spectrum and predicting seaway elevation response. What cannot be concluded from this particular work is the degree of optimality to which the eighth-order system can actually match the target spectrum. Thus far, based on history of previous studies in this area, the work conducted herein has indicated a promising direction for better predicting future seaway response. From this research, it is indicated that the eighth-order system allows adaptivity and a degree of future prediction capability based on past and current data.

## B. RECOMMENDATIONS

This filtering system is merely a baseline version for modeling seaway, the gain matrix for the innovator was not optimized. That is, the Linear Quadratic Regulator was not optimally chosen - the weighting matrices values were based on intuition drawn from past experiences without access to experimental data. If the Q and R matrices are chosen the predictor would most likely predict further into the future with more accuracy. Also, the ability of the prediction model to be adapted to seaway spectra that vary in peak frequency and frequency spread should be explored.

Also, it should be noted that the P-M target spectrum is recognized as an asymptotic form and it has some limitations, for shallow water applications. Therefore, the Bretschneider spectrum, which belongs to a two parameter spectrum family that permits period and wave height to be assigned separately, should be considered for future research.

## LIST OF REFERENCES

- Faltinsen, O.M., *Sea Loads on Ships and Offshore Structures*, Cambridge University Press, 1990.
- Hudspeth, R.T., and Borgman, L.E., "Efficient FFT Simulation of Digital Time Sequences," *Journal of the Engineering Mechanics Division*, ASCE, Vol. 105, No. EM2, Apr., 1979, pp. 223-235.
- Hunt, L.M., COMMINEWARCOM JOINT COUNTERMINE ACTD PHASE III, *Report to Commander, Mine Warfare Command*, Dec., 1995.
- Papoulias, F.A., "Dynamics of Marine Vehicles," *Informal Lecture Notes for ME 4823*, Summer 1993.
- Pierson, W.J., and Moskowitz, L., "A Proposed Spectral Form for Fully Developed Wind Seas Based on the similarity Theory of S. A. Kitaigorodskii," *Journal of Geophysical Research*, Vol. 69, No. 24, 1964, pp. 5181-5190.
- Richwine, D.A., "Forward . . . From the Sea. The Mine Warfare Implications," *Proceedings of the Autonomous Vehicles in Mine Countermeasures Symposium*, Monterey, CA, p. 2-1-2-6, April 1995.
- Sarpkaya, T., and Isaacson, M., *Mechanics of Wave Forces on Offshore Structures*, Van Nostrand Reinhold Company Inc., 1981.
- Shinozuka, M., "Monte Carlo Solution of Structural Dynamics," *Computers and Structures*, Vol. 2, 1972, pp. 855-874.
- Shinozuka, M., and Wai, P., "Digital Simulation of Short-Crested Sea Surface Elevations," *Journal of Ship Research*, Vol. 23, No. 1, Mar., 1979, pp. 76-84.
- Spanos, P-T.D., "ARMA Algorithms for Ocean Wave Modeling," *ASME Journal of Energy Resources Technology*, Vol. 105, Sept., 1983, pp. 300-309.
- Spanos, P-T.D., *Probabilistic Offshore Mechanics*, Computational Mechanics Inc., 1985.
- Spanos, P-T.D., and Hansen, J.E., "Linear Prediction Theory for Digital Simulation of Sea Waves," *ASME Journal of Energy Resources Technology*, Vol. 103, Sept., 1981, pp. 243-249.

Spanos, P-T.D., and Mignolet, M.P. "Z-Transform Modeling of P-M Wave Spectrum," *Journal of Engineering Mechanics*, Vol. 112, No 8, Aug., 1986, pp. 745-759.

## APPENDIX: EIGHTH-ORDER FILTER

```

function [rho] = predict(delta)
%       Matlab script to function as a Eighth-Order Digital Filter for
%       Predicting Future Seaway Elevation Response
%       Tracks and matches Pierson Moskowitz/Pressure Profile
%       Spectrum and predicts responses one full wave length
%
%       Variables
%       h = Fignificant wave height
%       w = Frequency
%       S = Defines Pierson Moskowitz expression for fully developed seas
%       t = Time vector
%       zeta = Damping ratio
%       T = Period interval
%       A,B = Continuous plant model
%       Phi,Gamma = Discrete plant model
%       K = Filter Gains
%       error=
%       x2 = Estimate of state vector
%       Y = System's output
%       rho = Cross-correlation coefficient
%       delta is the number of time steps, (i.e. Phi is delta minus one)
%

h=3;
w=[0.3:0.05:3];dw=0.05;
[l,ms]=size(w);
S=w;
for i=1:ms
    S(i)=8.1e-3*32.2^2/(w(i)^5)*exp(-33.56/h^2/(w(i)^4));
end;
ws=[0.3:0.05:3];

lambda=[171.61,146.52,127.62,112.86,100.98,91.21,83.01,76.02,70.64,73,...
60.08,55.94,52.23,48.88,45.83,43.05,40.49,38.14,35.96,33.93,32.05,30.29,...
28.64,27.1,25.66,24.3,23.03,21.84,20.71,19.66,18.67,17.75,16.88,16.07,15.30,...
14.59,13.92,13.29,12.7,12.15,11.63,11.15,10.69,10.26,9.86,9.47,9.11,8.77,...
8.45,8.15,7.86,7.59,7.33,7.08,6.85];

%       Pressue Measurement Simulation

lambda=lambda.*3.28;
t=[0:0.1:200];
Y=zeros(1,length(t));
for i=1:length(ws);
    phi=rand(1,length(ws));phi=phi-mean(phi);
    y(i,:)=(cosh(6*pi/lambda(i))/cosh(40*pi/lambda(i)))...
*(sqrt(S(i)*2*dw))*cos(ws(i)*t+phi(i)*pi*2);
end;
    for j=1:length(ws);
        Y=Y+y(j,:);
    end;

%       Defines Coefficients of transfer function of Eighth-Order Filter

T=0.1;w0=1.28;zeta=0.4;
n=[1/w0,0];d=[(1/w0)^2,2*zeta/w0,1]; % Defines Fourth-Order Expression
num=conv(n,n);num4=conv(num,num);
den=conv(d,d);den4=conv(den,den); % Defines transfer function

%       Defines innovater gains for subject filter

```

```

[A1,B1,C1,D1]=tf2ss(num4,den4);
[Phi,Gamma]=c2d(A1,B1,T);
K=dlqr(Phi',C1', eye(8,8)*10,.1); eig1=abs(eig(Phi-K'*C1))
x2=zeros(8,length(t));x4=x2;P2=zeros(1,length(t));P6=P2;

%       For loop for closed loop filter
for i=1:length(t)
    x2(:,i+1)=(Phi)*x2(:,i)+K'*(Y(i)-C1*x2(:,i));
    x60(:,i+1)=(Phi^delta)*x2(:,i+1);
    P2(i)=C1*x2(:,i);
    P60(i)=C1*x60(:,i);
end;

for i=1:(length(t)-delta);
    error60(i)=(P60(i)-Y(i+delta));Y60(i)=Y(i+delta);
end;

%       Calculates cross-correlation coefficient between P-M spectrum and filter
rho=(Y60*P60(1:(2001-delta))'/(std(Y60)*std(P60)))/(2001-delta);

```

## INITIAL DISTRIBUTION LIST

1. Defense Technical Information Center ..... 2  
8725 John J. Kingman Rd, STE 0944  
FT. Belvoir, VA 22060-6218
  
2. Dudley Knox Library ..... 2  
Naval Postgraduate School  
411 Dyer Rd  
Monterey, CA 93943-5101
  
3. Dr. Terry R. McNelly ..... 1  
Chairman, Mechanical Engineering Department  
Naval Postgraduate School  
Monterey, CA 93943-5000
  
4. Dr. Anthony J. Healey ..... 2  
Code ME/Hy  
Mechanical Engineering Department  
Naval Postgraduate School  
Monterey, CA 93943-5000
  
5. Curricular Office, Code 34 ..... 1  
Naval Postgraduate School  
Monterey, CA 93943-5000
  
6. LT Anthony L. Simmons ..... 2  
P. O. Box 548  
Goodwater, AL 35072
  
7. Dr. Dana Yoerger ..... 1  
Woods Hole Oceanographic Institution  
Deep Submergence Laboratory  
Woods Hole, MA 02543

- 8. Office of Naval Research (Code 321RS) ..... 1  
 800 North Quincy Street  
 Arlington, VA 22217-5660
  
- 9. Commander, Mine Warfare Command (Code 02R) ..... 1  
 325 5th Street SE  
 Corpus Christi, TX 78419
  
- 10. Dr. Samuel M. Smith ..... 1  
 Department of Ocean Engineering  
 Florida Atlantic University  
 500 NW 20th Street  
 Boca Raton, FL 33431-0991
  
- 11. Jim Bellingham ..... 1  
 MIT Sea Grant Program  
 MIT  
 Cambridge, MA 02139